IEEE Access
Multidisciplinary | Rapid Review | Open Access Journal

Received November 19, 2019, accepted December 27, 2019, date of publication January 13, 2020, date of current version January 22, 2020.

Digital Object Identifier 10.1109/ACCESS.2020.2966070

Positioning in a Multipath Channel Using OFDM Signals With Carrier Phase Tracking

HAN DUN[1], CHRISTIAN C. J. M. TIBERIUS[1], AND GERARD J. M. JANSSEN[2]
[1]Geoscience and Remote Sensing, Delft University of Technology, 2628 Delft, The Netherlands
[2]Circuits and Systems, Delft University of Technology, 2628 Delft, The Netherlands

Corresponding author: Han Dun (h.dun@tudelft.nl)

This work was supported by the Netherlands Organization for Scientific Research (NWO) through the project SuperGPS under Grant 13970.

ABSTRACT In developing a high accuracy terrestrial radio navigation system, as a complement to a global navigation satellite system (GNSS), it is recognized that the performance of time delay estimation is proportional to, and thereby limited by, the signal bandwidth. Given a possibly narrow signal bandwidth, the central carrier phase can, alternatively, provide a better distance accuracy, though the central carrier phase cycle ambiguity should be resolved. In practice, the carrier phase may be perturbed by multipath. In this paper, considering an orthogonal frequency division multiplexing (OFDM) signal, we propose a two-step carrier phase estimation method to reduce the error introduced by multipath. First, the propagation delay of the LoS path is coarsely determined, then the carrier phase is estimated using the earlier determined coarse time delays. Furthermore, a positioning model only based on carrier phase estimates is presented in this paper. The proposed technique is evaluated by statistical analyses and a simulated OFDM-based terrestrial positioning system in different roadway multipath environments. The results show that the impact of multipath on carrier phase estimation can be largely mitigated, so that the carrier phase can be used for precise positioning. In addition, fixing the integer carrier phase cycle ambiguities can significantly reduce the time for the position solution to converge to high precision.

INDEX TERMS Multipath channels, OFDM, phase estimation, radio navigation, multipath mitigation, phase ambiguity.

I. INTRODUCTION

Global navigation satellite systems (GNSS) have an excellent proven track record and a very high economic value, but also a number of limitations. Their performance is especially sensitive to multipath, atmospheric distortions and jamming [1], [2]. Recently, terrestrial positioning systems have been broadly studied as a complement to GNSS, or as an alternative approach for positioning and navigation [3]–[9]. Orthogonal frequency division multiplexing (OFDM) signals have been frequently referred to as an opportunistic signal that can be modified for terrestrial radio positioning. They can be found in various telecommunication systems, such as digital video broadcasting terrestrial (DVB-T) [3], [4], IEEE 802.11 a/g/p [5], [6], 4G/LTE [7], [8] and 5G [9]. Compared with GNSS, OFDM-based terrestrial systems are less affected by atmospheric errors, and can be easily installed in GNSS-challenged environments, such as indoor and in urban canyons.

Positioning directly based on the propagation time delay from OFDM signals requires relatively accurate time-of-arrival (ToA) estimation. The timing resolution is inversely proportional to the signal bandwidth. However, most existing OFDM-based systems only have a relatively narrow signal bandwidth (e.g., 10-100 MHz). Makki [10] proposed a two-step ToA estimation method based on OFDM signals: a coarse ToA estimation based on cross correlation, and a fine adjustment based on channel estimation. A sub-meter accuracy is achieved in an environment with little multipath interference. Besides, considering the impact of multipath, subspace methods, such as estimation of signal parameters via rotational invariance techniques (ESPRIT) and multiple signal classification (MUSIC) [11], have been also applied for time delay estimation. Because the delays of

The associate editor coordinating the review of this manuscript and approving it for publication was Yunlong Cai.

distinguishable paths in a multipath channel are estimated by a subspace-based method [12]–[14], the impact of multipath on time delay estimation of the direct line-of-sight (LoS) component can be largely mitigated. However, given a relatively narrow signal bandwidth, the LoS component may not be separable from close-in multipath. Consequently, ranging based on a subspace method can only achieve a meter-level accuracy.

On the other hand, as in GNSS, exploiting the phase measurement from the central carrier which is referred to as the *carrier phase* in this paper, can further improve positioning performance. Given an RF signal with a fixed signal bandwidth, the central carrier phase can provide a much better distance accuracy due to its small carrier wavelength, although unknown phase cycle ambiguities need to be resolved. In [15], Yang et al. analyzed carrier phase tracking of DVB-T signals. Since the middle subcarrier (i.e., DC component) is retained and assigned as a continuous pilot subcarrier, the carrier phase can be tracked without phase discontinuity. Khalife and Kassas [16] also demonstrate a precise UAV navigation system with sub-meter level accuracy using LTE carrier phase measurement, which is obtained by integrating the Doppler offset over the observation period [17], [18]. However, the aforementioned approaches assume that the received signals do not suffer from severe multipath.

In practice, multipath is present in most positioning scenarios. Since Doppler frequency offset estimation will be affected by multipath, the carrier phase derived from the Doppler frequency will be consequently perturbed. The carrier phase on the continual subcarriers (e.g., the DC subcarrier or pilots with constant data modulation) will be also affected by a multipath channel. Then, the carrier phase measurement becomes very sensitive to multipath. Especially, in a non-static scenario, the carrier phase can be easily perturbed by the time-variant multipath channel, and the phase error due to multipath can even vary beyond the interval -π to π. So that a time series of phase estimates can no longer be properly unwrapped.

Hence, in this paper a two-step carrier phase estimation approach is proposed to mitigate resolvable multipath (with a relative delay of a reflection larger than one sample interval, in line with the existing vehicular channel models e.g., [19]). First, a subspace method (e.g., ESPRIT) is used to determine the propagation delay, in which the performance is restricted by the available pilot subcarriers and signal bandwidth. Then, the complex gain is estimated, based on the determined propagation delay of the LoS component, eventually providing the carrier phase information. Since the LoS component and the reflections have been coarsely identified in the first step, as a result, in the second step we can estimate the carrier phase for the LoS component, and largely reduce the additional phase error induced by the reflections.

This paper is organized as follows. Section II introduces the OFDM signal model in a non-static positioning scenario. Then, in section III, the proposed two-step carrier phase estimation is explained, and its performance is statistically analyzed. Afterwards, the positioning model only based on carrier phase estimates is presented in section IV. Section V shows simulation results of LoS carrier phase estimation and the positioning performance based on the proposed two-step method in different outdoor LoS multipath channels. Conclusions are drawn in section VI.

II. OFDM SIGNAL

Using the inverse fast Fourier transform (IFFT), an OFDM symbol is generated by modulating N complex data points on N sub-carriers. In order to combat inter-symbol interference (ISI) caused by a multipath channel, a guard interval (i.e., cyclic prefix, CP) with N_g samples is generally added to every OFDM symbol [20]. Therefore, there are $N_g + N$ samples in each OFDM symbol, and the n-th sample of the l-th OFDM symbol ($l \geq 0$) in baseband is given by

$$s_{bb}[n] = \frac{1}{N} \sum_{k=-N/2}^{N/2-1} c_{k,l} e^{j\frac{2\pi(l(N_g+N)+N_g+n)k}{N}},$$

$$n = \begin{cases} -N_g, \ldots, -1 & \text{(CP)} \\ 0, \ldots, N-1 & \text{(data)}, \end{cases}$$

where k denotes the subcarrier index, and $c_{k,l}$ denotes the l-th complex symbol modulated on the k-th sub-carrier, $j = \sqrt{-1}$, T_s denotes the sampling interval, Δf denotes the subcarrier spacing, and $f_k = k\Delta f$ with $\Delta f = 1/(NT_s)$.

After digital-to-analog conversion (DAC), the baseband OFDM signal $s_{bb}(t)$ is modulated on a carrier with frequency f_c. Hence, the passband OFDM signal $s_{pb}(t)$ can be expressed as

$$s_{pb}(t) = \Re\left\{ s_{bb}(t) e^{j2\pi f_c t} \right\},$$

where $\Re\{\cdot\}$ denotes the real part of a complex value.

At the receiver, the passband signal perturbed by the channel and the noise is down-converted to baseband. To simplify the notation, the randomness introduced by the noise is omitted here, but it will be introduced in section III.

$$r_{bb}(t) = 2\mathcal{F}_L\left\{ (s_{pb}(t) * h(t)) \cos(2\pi f_c t + \varphi_0) \right\} + j2\mathcal{F}_L\left\{ -(s_{pb}(t) * h(t)) \sin(2\pi f_c t + \varphi_0) \right\}, \quad (1)$$

where $\mathcal{F}_L$ denotes low pass filter operator, $(*)$ denotes convolution, $h(t)$ denotes the channel impulse response, and φ_0 denotes the constant carrier phase difference of the reference carriers between the transmitter and the receiver, and is referred to as the initial carrier phase offset in this paper.

In order to demodulate the received OFDM signal properly, time synchronization should be conducted to find the starting point of the FFT window covering an OFDM symbol, and the CP is removed. In addition, the carrier frequency offset (CFO) and sampling clock offset (SCO) [20] need to be estimated and compensated as precisely as possible. For the purpose of positioning, we are only interested in the carrier phase, or the change of the carrier phase caused by a Doppler frequency offset. In this paper, we restrict ourselves to the analysis and mitigation of the impact of multipath on carrier

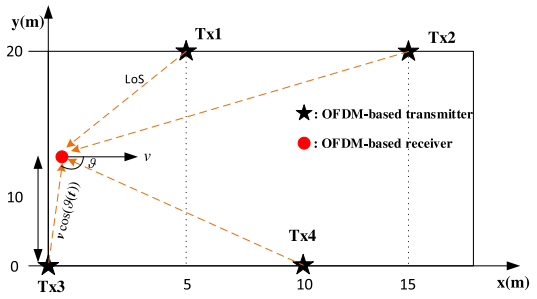

FIGURE 1. A 2-D roadway positioning scenario: four transmitters with fixed and known locations and one rover receiver moving with a speed of v, indicated by the black arrow.

phase estimation. A synchronized system is considered in the following sections, where the transmitters and receiver are assumed to share the same clock and frequency source. Consequently, the carrier frequency offset is only caused by the Doppler effect due to the movement of the receiver.

We start with a simple single-path channel and derive the received signal model. Then, the received signal in a multipath channel will be discussed.

A. SINGLE PATH CHANNEL

Considering an OFDM receiver in a non-static ranging scenario as shown in Fig. 1, the time-varying single-path propagation channel [21] can be modeled as

$$h(\tau, t) = \alpha(t)\delta(\tau - \tau_1(t)), \tag{2}$$

and t indicates the time when the channel response is observed by the receiver, $t - \tau$ indicates the time when the impulse is launched to the channel relative to the observation time t,

$$\tau_1(t) = \tau_1' - \int_0^t \frac{v\cos(\vartheta(v))}{c}\mathrm{d}v, \tag{3}$$

where $\delta(\cdot)$ denotes the Dirac function, τ_1' denotes the initial propagation delay at the start point (e.g. (0, 10) at time $t = 0$ in this example), $\vartheta(t)$ denotes the time-dependent angle-of-arrival of the LoS signal, c denotes the speed of light, and $[0,\ t]$ denotes the observation period, α denotes the signal amplitude gain due the propagation distance and the radio frequency. Over a relatively small scale positioning area or ranging distance, the change of α can be ignored. In addition, to simplify the notation, the speed of the receiver v is assumed constant, but it can be time variant in practice.

In addition, the propagation delay can be assumed constant across L OFDM symbols, as the change of the propagation delay in $L(N_g + N)T_s$ is much smaller than the temporal resolution T_s [12]. For example, considering a receiver moving with a speed of 80 km/h, the change of the propagation delay in $L = 20$ OFDM symbols (with $N_g = 16$, and $N = 64$ in an IEEE 802.11p-based system [22]) is $1.18 \times 10^{-4}T_s \ll T_s$.

For ease of notation, here we will neglect the constant carrier phase offset φ_0 shown in (1), but it will be introduced in the section IV. Thus, given a single path channel defined as in (2), the received baseband OFDM signal in (1) can be rewritten as

$$r_{bb}(t) = \alpha s_{bb}(t - \tau_1(t))e^{j2\pi f_c \tau_1(t)}. \tag{4}$$

According to (3), the instantaneous Doppler frequency shift [23] of the i-th sub-carrier at reception time t is given by

$$f_{D,k}(t) \approx (f_c + f_k)\frac{v\cos(\vartheta(t))}{c}, \quad \text{for } v \ll c. \tag{5}$$

As shown in (5), we can further assume that the Doppler frequency is constant during one OFDM symbol, since the signal arrival angle and the speed will not change significantly over one symbol (e.g., 6.4 μs). Thus, the instantaneous Doppler frequency shown in (5) can be rewritten as a function of the OFDM symbol index l, and approximated by

$$f_{D,k,l} = (f_c + f_k)\frac{v\cos(\vartheta_l)}{c} \approx f_c\frac{v\cos(\theta_l)}{c}, \tag{6}$$

Based on (6), after time synchronization and removing the CP, the received signal of the l-th symbol can be given as

$$\begin{aligned} r_{bb,l}[n] = \frac{\alpha}{N}\sum_{k=-N/2}^{N/2-1} c_{k,l}\exp\left(j\frac{2\pi kn}{N}\right) \\ \times \exp\left(-j2\pi((f_c + f_k)\tau_1' + f_{D,k,l}(N_g + n)T_s \right. \\ \left. + \phi_{D,k,l-1})\right), \quad n = 0, 1, \ldots, N-1, \end{aligned} \tag{7}$$

where $\phi_{D,k,l-1}$ denotes the cumulative change of the Doppler phase of the k-th subcarrier from the received RF signal in the previous $l - 1$ OFDM symbols, which is given by

$$\phi_{D,k,l-1} = \sum_{q=1}^{l-1} f_{D,k,q}(N_g + N)T_s, \quad l > 1. \tag{8}$$

With the bounds derived in [24], the inter-carrier interference due to Doppler can be neglected. After the FFT of (7), the received phasor on the k-th subcarrier in the l-th symbol can be written as

$$\begin{aligned} R_{k,l} &= \sum_{n=0}^{N-1} r_{bb,l}[n]\exp\left(-j2\pi\frac{kn}{N}\right) \\ &\approx \frac{\alpha}{N}c_{k,l}\exp\left(-j2\pi\left((f_c + f_k)\tau_1' + f_{D,k,l}N_gT_s \right.\right. \\ &\quad \left.\left. + \phi_{D,k,l-1}\right)\right)\sum_n \exp(-j2\pi f_{D,k,l}nT_s). \end{aligned} \tag{9}$$

Considering a sample rate T_s of 10^{-7} s, the term $f_{D,k,l}T_s$ in (9) is much smaller than one. If the Doppler frequency offset is less than 2000 Hz and the number of subcarriers N is much larger than one, we can have the following approximation,

$$\begin{aligned} &\sum_n \exp(-j2\pi f_{D,k,l}nT_s) \\ &= \frac{\sin\left(\pi f_{D,k,l}NT_s\right)}{\sin\left(\pi f_{D,k,l}T_s\right)}\exp\left(-j2\pi f_{D,k,l}\frac{(N-1)T_s}{2}\right) \\ &\approx N\exp(-j2\pi f_{D,k,l}NT_s/2). \end{aligned} \tag{10}$$

Afterwards, the received phasor in (9) is rewritten as

$$R_{k,l} \approx \alpha c_{k,l} \exp\left(-j2\pi \left((f_c + f_k)\tau_1' + f_{D,k,l}(N_g + N/2)T_s + \phi_{D,k,l-1}\right)\right). \quad (11)$$

Based on the approximation of the received phasor for the k-th subcarrier from the l-th symbol in (11), the instantaneous Doppler phase in the l-th symbol is approximately computed from $(N_g + N/2)$ samples.

B. MULTIPATH CHANNEL

So far, only a single path channel is considered. Although, we assume that the LoS path always exists, the channel may also contains multiple reflections with different propagation delays. Considering the channel impulse response given by

$$h(\tau, t) = \sum_{p=1}^{P} \alpha_p(t)\delta(\tau - \tau_p(t))$$
$$\boldsymbol{\tau}(t) = \begin{bmatrix}\tau_1(t) & \tau_2(t) & \dots & \tau_P(t)\end{bmatrix}, \quad (12)$$

in which P is the number of paths in a multipath channel, and α_p and $\tau_p(t)$ are the gain and the delay of the p-th path, respectively. Again, the gain α_p is assumed to be constant in a relatively small area. Similarly, the propagation delay is assumed to be quasi-stationary across L OFDM symbols. By default, $\tau_1(t)$ denotes the propagation delay of the direct LoS path.

Considering the propagation delay defined in (3), then, the received phasor in such a multipath condition can be written as

$$R_{k,l,mp} = R_{k,l} + \sum_{p=2}^{P} \alpha_p c_{k,l} \times \exp\left(-j\left(2\pi(f_c + f_k)\tau_p' + \varphi_{k,l}^{(p)}\right)\right), \quad (13)$$

where $R_{k,l,mp}$ denotes the received k-th subcarrier phasor from the l-th symbol in a multipath channel, $R_{k,l}$ denotes the received phasor of the LoS path on the k-th subcarrier shown in (11), τ_p' denotes the initial delay of the p-th path, and $\varphi_{k,l}^{(p)}$ denotes the cumulative Doppler phase of the p-th path. Unlike in telecommunication, our interest lies only in the LoS path.

III. TWO-STEP CARRIER PHASE ESTIMATION

For the purpose of ranging and positioning, the propagation time delay of the LoS path should be estimated as accurately as possible. The ESPRIT method has been studied for time delay estimation in a multipath channel [13]. The bias due to the multipath can be largely mitigated as compared to the classic matched-filter method. However, the performance of time delay estimation is still largely restricted by the signal bandwidth. Alternatively, as in GNSS, we can use the phase from the central carrier to retrieve the desired geometric information. Although using the carrier phase can improve the ranging accuracy, it can be also easily perturbed by multipath due to its short wavelength. In a multipath condition, the carrier phase can be derived from the received phasor, which is a sum of phasors for the LoS component and reflections. Considering a high central frequency, a certain small time variation can cause a large phase rotation on the phasor of each reflection.

In this section, a two-step carrier phase estimation approach is proposed to mitigate the impact of multipath. First, the ESPRIT method is applied to distinguish the LoS component and the multiple reflections as well as possible. Then, the propagation delay of the direct LoS path determined by the ESPRIT method is used to estimate the carrier phase in the second step. Consequently, positioning based on such a system can be robust in multipath conditions and also takes advantage of the small wavelength of the central carrier.

A. STEP 1: ESPRIT-BASED TIME DELAY ESTIMATION

Here we consider a P-path multipath channel in a non-static scenario as defined in (12). The channel response on each subcarrier can be estimated based on the received phasor (13), as long as the data modulated on each subcarrier (e.g., long training symbol) is known at the receiver [25]. Initially, we can use all subcarriers for ranging and positioning, but we can also only use some pilots such as comb-type pilots. In this section, we use N_p comb-type pilots with a spacing of Δp as a general case. When $\Delta p = 1$, then all subcarriers are used for ranging. The channel response estimated from the k-th pilot subcarrier is given as

$$H_{k,l} = R_{k,l,mp}/c_{k,l}$$
$$k \in [-N_p/2, -N_p/2 + 1, \dots, N_p/2 - 1]\Delta p \quad (14)$$

Then, the observation model of a non-static receiver for the l-th symbol is given by

$$\underline{\boldsymbol{H}}_l = A(\tau_{1,l}, \tau_{2,l}, \dots, \tau_{P,l})\boldsymbol{x}_l + \underline{\boldsymbol{n}}, \quad (15)$$

where the underscore $\underline{(\cdot)}$ denotes a random variable, $\underline{\boldsymbol{H}}_l$ is defined as

$$\begin{bmatrix}\underline{H}_{-N_p/2,l} & \dots & \underline{H}_{N_p/2-2,l} & \underline{H}_{N_p/2-1,l}\end{bmatrix}^{\mathrm{T}},$$

where $(\cdot)^{\mathrm{T}}$ denotes the transpose operator, $\tau_{p,l}$ denotes the propagation delay of the p-th path for the l-th symbol, which can vary from symbol to symbol. In addition, the $N_p \times 1$ vector $\underline{\boldsymbol{n}}$ contains the additive white Gaussian noise on each ranging pilot subcarrier, and the p-th column of the $N_p \times P$ matrix $A(\tau_{1,l}, \tau_{2,l}, \dots, \tau_{P,l})$ can be written as

$$\begin{bmatrix} \exp\left(-j(2\pi f_{-N_p/2}\tau_p' + \varphi_{-N_p/2,l}^{(p)})\right) \\ \exp\left(-j(2\pi f_{-N_p/2+1}\tau_p' + \varphi_{-N_p/2+1,l}^{(p)})\right) \\ \vdots \\ \exp\left(-j(2\pi f_{N_p/2-1}\tau_p' + \varphi_{N_p/2-1,l}^{(p)})\right) \end{bmatrix},$$

in which the frequency of the k-th pilot subcarrier is written as

$$f_k = k\Delta p \Delta f,$$

τ_p' denotes the initial delay of the p-th path (cf. (3)). In addition, the p-th element of the $P \times 1$ vector $\boldsymbol{x}_p$ is $\alpha_p \exp\left(-j(2\pi f_c \tau_p' + \varphi_{c,l}^{(p)})\right)$, and

$$\varphi_{k,l}^{(p)} = 2\pi f_{D,k,l}^{(p)}(N_g + N/2)T_s + \phi_{D,k,l-1}^{(p)},$$
$$\varphi_{c,l}^{(p)} = 2\pi f_{D,c,l}^{(p)}(N_g + N/2)T_s + \phi_{D,c,l-1}^{(p)},$$

where $f_{D,k,l}^{(p)}$ and $f_{D,c,l}^{(p)}$ denote the Doppler frequency shifts of the p-th path in the l-th symbol on the k-th pilot subcarrier f_k, and on the central carrier f_c, respectively. Unlike (8), $\phi_{D,k,l-1}^{(p)}$ is now defined as the cumulative Doppler phase from the previous $l-1$ symbols on the k-th pilot subcarrier, and $\phi_{D,c,l-1}^{(p)}$ is defined as the cumulative Doppler phase on the central carrier.

Generally, $f_{D,k,l}^{(p)}$ is much smaller than $f_{D,c,l}^{(p)}$, and its change over a certain number of symbols can be neglected, thus, we can assume that all subcarriers suffer from approximately the same Doppler shift. As also stated in section II. A, we can assume the propagation delay is constant across L symbols. Hence, we can assume that the design matrix A in (15) is approximately invariant over a reasonable amount of OFDM symbols, as long as the multipath profile and the positioning geometry do not change dramatically. Over a reasonable amount of OFDM symbols, the observation model (15) can be simplified as

$$\underline{\boldsymbol{H}}_l \approx A(\tau_1, \tau_2, \ldots, \tau_P)\boldsymbol{x}_l + \underline{\boldsymbol{n}}. \tag{16}$$

in which the symbol index l is removed in the design matrix A, but still remains in the observation $\underline{\boldsymbol{H}}_l$ and the unknown complex gain $\boldsymbol{x}_l$.

In order to implement the subspace method, the sample covariance matrix can be constructed from multiple OFDM symbols [12] as follows

$$\underline{Q} = \sum_{l=1}^{L} \underline{\boldsymbol{H}}_l \underline{\boldsymbol{H}}_l^{\mathrm{H}}, \tag{17}$$

where $(\cdot)^{\mathrm{H}}$ denotes the Hermitian transpose, L indicates the number of OFDM symbols, in which the design matrix A is assumed to be quasi-static as in (16). It is also worth to mention that given a finite duration of the observation (e.g., a single OFDM symbol), a snap-shot measurement can be reshaped into a Hankel matrix [13], then the sample covariance matrix can be derived based on the forward-backward approach [13], [26].

To describe the column span of matrix A with rank P shown in (16), a singular value decomposition of A can be used as [27]

$$A = U_s \Sigma_s V_s^{\mathrm{H}},$$

where U_s contains P orthonormal columns which span the column space of A, Σ_s denotes a $P \times P$ diagonal matrix containing the nonzero singular values of A, and V_s denotes a $P \times P$ unitary matrix.

In practice, matrix A is unknown, thus the subspace basis is derived from the SVD of the sample covariance matrix (17). In addition, using minimum description length (MDL) criteria [28], the number of paths P can be determined.

In order to implement the ESPRIT method, we should find a rotation invariant matrix. In this case, since N_p comb-type pilot subcarriers are used for ranging, and the spacing is the same across all pilots (i.e., $\Delta p \Delta f$). Hence we can select the first $N_p - 1$ rows A defined as $A^{(1)}$, also let the last $N_p - 1$ rows of A be denoted as $A^{(2)}$, and further have

$$A^{(2)} = A^{(1)}\Theta$$

where Θ denotes the rotation invariant matrix of A, which is a diagonal matrix and can be written as

$$\Theta = \mathrm{diag}([\exp(-j2\pi\,\Delta p \Delta f\,\tau_1),\ \ldots,\ \exp(-j2\pi\,\Delta p \Delta f\,\tau_{P-1}),\ \exp(-j2\pi\,\Delta p \Delta f\,\tau_P)]). \tag{18}$$

Hence, there should be a $P \times P$ invertible projection matrix T that maps one basis to the other, thus we have

$$U_s^{(1)} = A^{(1)}T, \quad U_s^{(2)} = A^{(2)}T = A^{(1)}\Theta T, \tag{19}$$

where $U_s^{(1)}$ and $U_s^{(2)}$, respectively, denote the first $N_p - 1$ rows of A and the last $N_p - 1$ rows of U_s. Based on (19), we have

$$U_s^{(2)} = U_s^{(1)}\left(T^{-1}\Theta T\right). \tag{20}$$

Hence, the solution of (20) can be derived based on a total least squares (TLS)-LS algorithm [27] as

$$\underbrace{\left(U_s^{(1)\mathrm{H}}U_s^{(1)}\right)^{-1}U_s^{(1)\mathrm{H}}U_s^{(2)}}_{D} = T^{-1}\Theta T, \tag{21}$$

which indicates that the eigenvalues of the matrix D will be the diagonal elements of the rotational invariant matrix Θ. Then, the propagation time delays of each path can be derived from the phases of the eigenvalues.

The rotational invariant matrix Θ is related to the column space of A, so the central frequency f_c is captured in P-vector $\boldsymbol{x}_l$ instead. Therefore, the phase of the diagonal elements in Θ are determined by the propagation delay and the pilot spacing (i.e., $\Delta p \Delta f$) which is much smaller than the actual central carrier frequency f_c. Consequently, the performance of the solution only relies on the spacing of the pilot sub-carriers $\Delta p \Delta f$ instead of the central carrier frequency f_c.

For an OFDM system with 64 sub-carriers and a 10 MHz bandwidth, the spacing Δf is 156.25 kHz in (18). When all subcarriers are allocated as pilots (i.e., $N_p = N = 64$, $\Delta p = 1$), and the propagation delay of each path is less than the period $1/\Delta f$, which is equivalent to 1920 m in distance, we can derive the propagation delay unambiguously from the phase. Similarly, if we only use $N_p = 16$ comb-type pilots with $\Delta p = 4$ for positioning, we can unambiguously determine the propagation delay when the propagation distance is less than 480 m. Therefore, as long as the propagation delay is less than $1/(\Delta p \Delta f)$, no phase cycle ambiguity problem will be encountered in the ESPRIT method.

B. STEP 2: LOS CARRIER PHASE ESTIMATION

Now, the design matrix A in (16) can be constructed based on the time delays derived from the ESPRIT method. To simplify the notation, the symbol index l is omitted here, but it will be introduced again in section IV. The complex gain $\boldsymbol{x}$ in every OFDM symbol, which contains the carrier phase information, can be computed based on least-squares estimation (LSE) as follows

$$\hat{\underline{\boldsymbol{x}}} = (A^{\mathrm{H}}(\hat{\underline{\tau}}_1, \hat{\underline{\tau}}_2, \ldots \hat{\underline{\tau}}_P)A(\hat{\underline{\tau}}_1, \hat{\underline{\tau}}_2, \ldots \hat{\underline{\tau}}_P))^{-1} A^{\mathrm{H}}(\hat{\underline{\tau}}_1, \hat{\underline{\tau}}_2, \ldots \hat{\underline{\tau}}_P)\underline{\boldsymbol{H}}. \quad (22)$$

In practice, if subcarriers experience different fading (i.e., have different SNR), best linear unbiased estimation (BLUE) instead of unweighted-LSE should be applied.

Since we assume that the propagation delay of the LoS path always has the smallest value among all estimated time delays, we can simply compute the LoS carrier phase from the first component of $\boldsymbol{x}$ denoted as x

$$\underline{\Phi} = \arg(\hat{\underline{x}}). \quad (23)$$

In (22), the design matrix A is constructed based on the propagation delay of each path to estimate the complex gain $\boldsymbol{x}$. However, it may not be necessary to fully retrieve the entire channel. Here, we only consider a 2-path channel as an example to illustrate the impact of the design matrix A on carrier phase estimation, but this can be easily extended to a channel that contains more than two paths. Initially, we use all subcarriers for phase estimation. Alternatively, we can also use only a few pilots to estimate the carrier phase, as long as we can still estimate the most significant reflections in a multipath channel and reconstruct the design matrix A in (22).

First, we analyze the estimators' variance matrix in (22) based on N_p comb-type pilots, which is computed as follows

$$\begin{aligned}
&\left(A^{\mathrm{H}}(\hat{\underline{\tau}}_1, \hat{\underline{\tau}}_2)A(\hat{\underline{\tau}}_1, \hat{\underline{\tau}}_2)\right)^{-1} \\
&= \frac{1}{N_p}\begin{bmatrix} T(0) & T(\hat{\underline{\tau}}_{2,1}) \\ T(\hat{\underline{\tau}}_{2,1})^* & T(0) \end{bmatrix}^{-1} \\
&= \frac{1}{N_p\left(|T(0)|^2 - |T(\hat{\underline{\tau}}_{2,1})|^2\right)}\begin{bmatrix} T(0) & -T(\hat{\underline{\tau}}_{2,1})^* \\ -T(\hat{\underline{\tau}}_{2,1}) & T(0) \end{bmatrix},
\end{aligned} \quad (24)$$

where $(\cdot)^*$ stands for the complex conjugate operation, $|\cdot|$ denotes the modulus operator, $\tau_{2,1}$ denotes the relative delay defined as

$$\tau_{2,1} = \tau_2 - \tau_1,$$

$|T(\cdot)|$ stands for the modulus of the summation of exponential functions and is given by

$$\begin{aligned}
|T(x)| &= \left|\frac{1}{N_p}\sum_{i=-N_p/2}^{N_p/2-1}\exp\left(-j2\pi\frac{i\Delta p}{NT_s}x\right)\right| \\
&= \frac{1}{N_p}\left|\frac{\sin\left(2\pi\frac{\Delta p}{NT_s}\frac{N_p}{2}x\right)}{\sin\left(2\pi\frac{\Delta p}{NT_s}\frac{1}{2}x\right)}\right|,
\end{aligned} \quad (25)$$

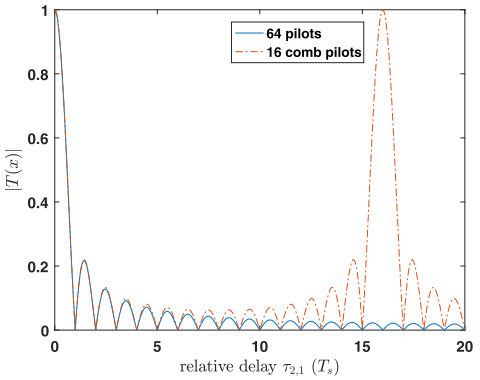

FIGURE 2. Modulus of the sum of exponential functions shown in (25), for the FFT size N is 64. Considering a 10 MHz signal bandwidth, the sampling interval T_S is 10^{-7}s. There are two curves, the blue solid-line represents the case of using all 64 pilots for carrier phase estimation, and the red dash-line represents the case of only using $N_p = 16$ comb-type pilots for estimation.

in which we assume that N_p comb-type pilot subcarriers with a uniform spacing of $\Delta p\Delta f$ are used for carrier phase estimation.

Fig. 2 shows the modulus of the summation of exponential functions for different relative delays $\tau_{2,1}$. Assuming that all subcarriers are allocated as pilots for positioning (blue solid line), if the LoS component and the reflection are well separated (e.g., $\tau_{2,1} \geq 0.8T_s$), $|T(\tau_{2,1})|$ in (24) will be much smaller than one (e.g., $|T(\tau_{2,1})| < 0.2$). Then, the variance matrix (24) is approximately diagonal.

On the other hand, if we only use $N_p = 16$ pilot subcarriers with $\Delta p = 4$, another main lobe will be at 16 T_s (see the read line in Fig.2). Considering a reflection with a relative delay of 16 T_s, then the variance matrix (25) becomes infinite, as $T(0) = T(16T_s)$. If the signal bandwidth is 10 MHz, another main lobe will appear at 1.6×10^{-7} s, which is equivalent to 480 m in distance. If the relative gain α of this reflection is less than 0.2, which will happen most of the time in practice, variance matrix (24) is approximately diagonal.

If there are more than two paths in a multipath channel, and the LoS is well separated from the reflections (e.g., $\tau_{p,1} \geq 0.8T_s$), the variance matrix derived in (24) can be approximated by a block diagonal matrix. It indicates that there is little correlation between the first estimator in (22) and the others.

In such a condition, the carrier phase can be simply estimated based on the LoS propagation delay or the first column of the design matrix A denoted as $\mathbf{a}(\hat{\underline{\tau}}_1)$. The complex gain of the LoS component can be computed as follows

$$\begin{aligned}
\hat{\underline{x}} &\approx \frac{1}{N_p}\mathbf{a}(\hat{\underline{\tau}}_1)^{\mathrm{H}}\underline{\boldsymbol{H}} \\
&= \alpha_1 T\left(\hat{\underline{\tau}}_1 - \tau_1\right)\exp\left(-j2\pi f_c\tau_1\right) \\
&\quad + \sum_{p=2}^{P}\alpha_p T\left(\hat{\underline{\tau}}_1 - \tau_p\right)\exp\left(-j2\pi f_c\tau_p\right) + \frac{\boldsymbol{a}(\hat{\underline{\tau}}_1)\underline{\boldsymbol{n}}}{N_p} \\
&\approx \alpha_1\exp(-j2\pi f_c\tau_1) + \frac{\boldsymbol{a}(\hat{\underline{\tau}}_1)\underline{\boldsymbol{n}}}{N_p}.
\end{aligned} \quad (26)$$

C. TIME SYNCHRONIZATION OFFSET

In reality, due to noise or multipath, we may not achieve a perfect time synchronization, which offsets the FFT window for channel estimation and data demodulation. This causes an extra delay on the received baseband signal. If no negligible inter-symbol interference occurs, after the FFT, an extra phase rotation will be present on each subcarrier and also the channel frequency response. Consequently, the propagation delay determined by the ESPRIT method will contain a bias due to a time synchronization offset.

A time synchronization offset, which is denoted as $\Delta\tau$, only causes an extra phase rotation on each subcarrier. We define the phase rotation matrix Ψ by

$$\Psi = \mathrm{diag}\left(\begin{bmatrix} \exp(-j2\pi f_{-N/2}\Delta\tau) \\ \exp(-j2\pi f_{-N/2+1}\Delta\tau) \\ \vdots \\ \exp(-j2\pi f_{N/2-1}\Delta\tau) \end{bmatrix}\right). \tag{27}$$

Then, the complex gain in (26) can be rewritten as

$$\begin{aligned} \hat{\underline{x}} &= \frac{1}{N}\boldsymbol{a}(\hat{\underline{\tau}}_1 + \Delta\tau)^{\mathrm{H}}\underline{\boldsymbol{H}}' \\ &= \frac{1}{N}\boldsymbol{a}(\hat{\underline{\tau}}_1 + \Delta\tau)^{\mathrm{H}}\Psi\underline{\boldsymbol{H}} \\ &= \frac{1}{N}\left(\Psi a(\hat{\underline{\tau}}_1)\right)^{\mathrm{H}}\Psi\underline{\boldsymbol{H}} = \frac{1}{N}a(\hat{\underline{\tau}}_1)^{\mathrm{H}}\underline{\boldsymbol{H}}, \end{aligned} \tag{28}$$

where $\underline{\boldsymbol{H}}'$ is the channel response affected by the time synchronization offset, and can be obtained from (14). Although a time synchronization offset causes a bias in the propagation delay determined by the ESPRIT method, its impact can be fully eliminated in carrier phase estimates as $\Psi^{\mathrm{H}}\Psi = \mathrm{I}$. Since both the design matrix A and the observations $\boldsymbol{H}'$ in (28) contain this bias, the estimate of unknown gain x can be still unbiased.

D. PERFORMANCE ANALYSIS

Now, we analyze the impact of using only the first column of matrix A in (16), denoted by $\boldsymbol{a}(\tau_1)$, to estimate the carrier phase, when there is no close-in multipath. Moreover, without loss of generality, N_p comb-type pilots with a spacing of Δp are considered in this section. If Δp is set to one, then all $N = N_p$ subcarriers are used for carrier phase estimation.

The random vector of variables $\underline{\boldsymbol{n}}$ in (15) is assumed to stem from zero-mean Gaussian noise, thus, the elements in $\underline{\boldsymbol{n}}$ also satisfy a zero-mean complex Gaussian distribution [29] and are identically distributed for each subcarrier, which can be denoted as

$$\begin{bmatrix} \Re\{\underline{n}_k\} \\ \Im\{\underline{n}_k\} \end{bmatrix} \sim \mathcal{N}\left(\begin{bmatrix} 0 \\ 0 \end{bmatrix}, \begin{bmatrix} \sigma_n^2 & 0 \\ 0 & \sigma_n^2 \end{bmatrix}\right), \tag{29}$$

where $\underline{n}_k$ denotes the measurement noise on the k-th subcarrier, $\Im$ and $\Re$ respectively represent the imaginary and real part of a complex value.

In order to estimate the LoS carrier phase from the complex gain x as derived in (26), the design matrix must be known. In our proposed approach, τ_1 in (26) is coarsely determined in the first step, so that the design matrix can be constructed. For the purpose of clarity, instead of using the notation $\hat{\underline{\tau}}_1$, a random variable $\hat{\underline{\delta}}$ is introduced here to explicitly denote the random time delay error,

$$\hat{\underline{\tau}}_1 = \tau_1 + \hat{\underline{\delta}}$$

However, to simplify the notation, we replace $\hat{\underline{\delta}}$ by $\underline{\delta}$ in the following derivation. It is assumed to satisfy a Gaussian distribution $\underline{\delta} \sim \mathcal{N}(\delta, \sigma_\delta^2)$. The mean value δ may not be zero, due to a residual multipath error. The time delay error is caused by multipath and thermal noise. Hence, the time delay error $\underline{\delta}$ and the noise $\underline{n}_k$ will be correlated.

Consequently, the design matrix $\boldsymbol{a}(\hat{\underline{\tau}}_1)$ in (26) including the time delay error can be written as

$$\mathbf{a}(\tau_1, \underline{\delta}) = \begin{bmatrix} \exp(-j2\pi f_{-N_p/2}(\tau_1 + \underline{\delta})) \\ \exp(-j2\pi f_{-N_p/2+1}(\tau_1 + \underline{\delta})) \\ \vdots \\ \exp(-j2\pi f_{N_p/2-1}(\tau_1 + \underline{\delta})) \end{bmatrix}. \tag{30}$$

Now, the complex gain x can be computed based on ordinary (un-weighted) least squares estimation, and is given by

$$\begin{aligned} \hat{\underline{x}} &= (\mathbf{a}(\tau_1, \underline{\delta})^{\mathrm{H}}\mathbf{a}(\tau_1, \underline{\delta}))^{-1}\mathbf{a}(\tau_1, \underline{\delta})^{\mathrm{H}}\underline{\boldsymbol{H}} \\ &= \alpha \exp(-j2\pi f_c\tau_1)|T(\underline{\delta})| \exp\left(-j\pi\,\Delta p\Delta f\,\underline{\delta}\right) \\ &\quad + \frac{1}{N_p}\sum_{k=-N_p/2}^{N_p/2-1} \exp(j2\pi f_k(\tau_1 + \underline{\delta}))\underline{n}_k. \end{aligned} \tag{31}$$

The derivation of (31) can be found in Appendix A. If the error $\underline{\delta}$ is relatively small (e.g., $\sigma_\delta \leq 0.2\ T_s$, or at few meter-level in distance, considering a 10 MHz bandwidth), $|T_p(\underline{\delta})|$ can be approximated to one.

The time delay error $\underline{\delta}$ and the noise $\underline{n}_i$ are functionally dependent in (31), which causes some complexities in error propagation. As a substitute, for the purpose of the statistical analysis, we consider the following relation

$$f_{\underline{\gamma}}(\underline{\delta}, \underline{n}_k) \approx f_{\underline{\nu}}(\underline{n}_k), \tag{32}$$

where $f_{\underline{\gamma}}$ and $f_{\underline{\nu}}$ denote the PDF of $\underline{\gamma}$ and $\underline{\nu}$ respectively, which are replaced by

$$\underline{\gamma} = \frac{1}{N_p}\sum_{k=-N_p/2}^{N_p/2-1} \exp(j2\pi f_k(\tau_1 + \underline{\delta}))\underline{n}_k, \quad \underline{\nu} = \frac{1}{N_p}\sum_{k=-N_p/2}^{N_p/2-1} \underline{n}_i.$$

The validation of the approximation (32) can be found in Appendix B.

Therefore, for the statistical analysis, equation (31) can be replaced by

$$\begin{aligned} \hat{\underline{x}} &\approx \alpha \exp(-j2\pi f_c\tau_1) \exp\left(-j2\pi\,\Delta p\Delta f\,\frac{\underline{\delta}}{2}\right) + \underline{\nu} \\ &= \underline{\gamma} + \underline{\nu}, \end{aligned} \tag{33}$$

where $\underline{\gamma}$ denotes the carrier component only perturbed by the time delay error $\underline{\delta}$, and $\underline{\nu}$ denotes the error component due to the noise $\underline{\boldsymbol{n}}$.

First, the distribution of $\underline{\nu}$ can be derived from (29) by utilizing the linear variance propagation law, and assuming that the noise on every subcarrier is identically distributed,

$$\begin{bmatrix}\Re\{\underline{\nu}\}\\ \Im\{\underline{\nu}\}\end{bmatrix} \sim \mathcal{N}\left(\begin{bmatrix}0\\0\end{bmatrix}, \begin{bmatrix}\frac{\sigma_n^2}{N_p} & 0\\ 0 & \frac{\sigma_n^2}{N_p}\end{bmatrix}\right). \tag{34}$$

In order to compute the phase, the argument of $\hat{\underline{x}}$ in (33) can be derived as

$$\begin{aligned}\underline{\Phi} &= \arg\left(\frac{\Im(\underline{\gamma}+\underline{\nu})}{\Re(\underline{\gamma}+\underline{\nu})}\right)\\ &\approx \arg\left(\frac{\Im(\underline{\gamma})}{\Re(\underline{\gamma})}\right) + \arg\left(\frac{|P_{\underline{\gamma}}^{\perp}\underline{\nu}|}{|\underline{\gamma}|+|P_{\underline{\gamma}}\underline{\nu}|}\right),\end{aligned} \tag{35}$$

where $P_{\underline{\gamma}}\underline{\nu}$ and $P_{\underline{\gamma}}^{\perp}\underline{\nu}$ are orthogonal projectors, $P_{\underline{\gamma}}\underline{\nu}$ is produced by projecting $\underline{\nu}$ onto $\underline{\gamma}$, and $P_{\underline{\gamma}}^{\perp}\underline{\nu}$ is generated by projecting $\underline{\nu}$ along the orthogonal complement of $\underline{\gamma}$. Since

$$\arg\left(\frac{\Im(\underline{\gamma})}{\Re(\underline{\gamma})}\right) = \left(-2\pi f_c\tau_1 - 2\pi\,\Delta p\Delta f\frac{\delta}{2}\right) \mod(-\pi,\pi],$$

for instance obtained through the arctan, and if the bias term is much less than 2π (i.e., $\Delta p\Delta f\frac{\delta}{2} \ll 1$), then we can have

$$\arg\left(\frac{\Im(\underline{\gamma})}{\Re(\underline{\gamma})}\right) = \underline{\theta} \approx (-2\pi f_c\tau_1 \mod(-\pi,\pi]) - 2\pi\,\Delta p\Delta f\frac{\delta}{2},$$

and equation (35) can be written as

$$\underline{\Phi} \approx \underline{\theta} + \arg\left(\frac{|P_{\underline{\gamma}}^{\perp}\underline{\nu}|}{|\underline{\gamma}|+|P_{\underline{\gamma}}\underline{\nu}|}\right). \tag{36}$$

Now we can analyze the second term with the argument function in (36). In order to derive the variance of $P_{\underline{\gamma}}^{\perp}\underline{\nu}$, we can apply the coordinate transformation

$$\begin{bmatrix}|P_{\underline{\gamma}}\underline{\nu}|\\ |P_{\underline{\gamma}}^{\perp}\underline{\nu}|\end{bmatrix} = \begin{bmatrix}\cos(\underline{\theta}) & \sin(\underline{\theta})\\ -\sin(\underline{\theta}) & \cos(\underline{\theta})\end{bmatrix}\begin{bmatrix}\Re(\underline{\nu})\\ \Im(\underline{\nu})\end{bmatrix}.$$

We can observe that it is difficult to derive the variance of the projection due to the non-linear function of $\underline{\theta}$ in the transformation matrix. However, considering a standard deviation of the time delay error of $\sigma_\delta \leq 0.2\,T_s$ and the subcarrier spacing being $\Delta f = 1/NT_s$, and all subcarriers being used for estimation (i.e., $\Delta p = 1$), the standard deviation of θ is about $0.2\pi/N \approx 0.01$ rad. Thus, we can have the following approximation

$$\begin{bmatrix}|P_{\underline{\gamma}}\underline{\nu}|\\ |P_{\underline{\gamma}}^{\perp}\underline{\nu}|\end{bmatrix} \approx \begin{bmatrix}\cos(\theta) & \sin(\theta)\\ -\sin(\theta) & \cos(\theta)\end{bmatrix}\begin{bmatrix}\Re(\underline{\nu})\\ \Im(\underline{\nu})\end{bmatrix}, \tag{37}$$

and

$$|P_{\underline{\gamma}}^{\perp}\underline{\nu}| \approx -\sin(\theta)\Re(\underline{\nu}) + \cos(\theta)\Im(\underline{\nu}). \tag{38}$$

Moreover, when the SNR is relatively large, and as long as the time delay error $\underline{\delta}$ is not an integer multiple of the sample interval (i.e., $|T_p(\underline{\delta})| \neq 0$, otherwise the signal will become zero), then in (36) we have

$$|\underline{\nu}|^2 \ll |\underline{\gamma}|^2,$$

where $\underline{\nu}$ stems from the noise $\underline{\boldsymbol{n}}$ with zero mean and its variance is reduced by a factor of N_p. To simplify the denominator of (36), we can make the approximation

$$|\underline{\gamma}| + |P_{\gamma}\underline{\nu}| \approx |\underline{\gamma}| = \alpha.$$

In addition, since $|P_{\underline{\gamma}}^{\perp}\nu|/|\underline{\gamma}| \ll 1$, equation (36) can be simplified as

$$\begin{aligned}\underline{\Phi} &\approx \underline{\theta} + \arg\left(\frac{|P_{\underline{\gamma}}^{\perp}\underline{\nu}|}{|\underline{\gamma}|}\right) \approx \underline{\theta} + \frac{|P_{\underline{\gamma}}^{\perp}\underline{\nu}|}{|\underline{\gamma}|}\\ &\approx (-2\pi f_c\tau_1 \mod(-\pi,\pi]) - \pi\,\Delta p\Delta f\underline{\delta}\\ &\quad - \frac{\sin(\theta)}{\alpha}\Re(\underline{\nu}) + \frac{\cos(\theta)}{\alpha}\Im(\underline{\nu}).\end{aligned} \tag{39}$$

Hence, the variance of the carrier phase estimator can be derived from the linear variance propagation law [30],

$$\sigma_\Phi^2 = FQF^{\mathrm{T}} \tag{40}$$

where F is given by

$$F = \left[\pi\,\Delta p\Delta f,\ -\frac{\sin(\theta)}{\alpha},\ \frac{\cos(\theta)}{\alpha}\right]$$

and the variance matrix Q of the random variables in (39) is written as

$$Q = \begin{bmatrix}\sigma_\delta^2 & \sigma_{\delta\Re(\nu)} & \sigma_{\delta\Im(\nu)}\\ \sigma_{\Re(\nu)\delta} & \sigma_{\Re(\nu)}^2 & 0\\ \sigma_{\Im(\nu)\delta} & 0 & \sigma_{\Im(\nu)}^2\end{bmatrix}.$$

Since the time delay error also stems from the noise, thus the covariance $\sigma_{\delta\Re(\nu)}$ and $\sigma_{\delta\Im(\nu)}$ will not likely be zero. Consequently, the variance σ_Φ^2 can be derived as

$$\begin{aligned}\sigma_\Phi^2 &= (\pi\,\Delta p\Delta f)^2\sigma_\delta^2 - 2\pi\,\Delta p\Delta f\frac{\sin(\theta)}{\alpha}\sigma_{\delta\Re(\nu)}\\ &\quad + 2\pi\,\Delta p\Delta f\frac{\cos(\theta)}{\alpha}\sigma_{\delta\Im(\nu)} + \frac{\sin^2(\theta)}{\alpha^2}\sigma_{\Re(\nu)}^2\\ &\quad + \frac{\cos^2(\theta)}{\alpha^2}\sigma_{\Im(\nu)}^2\end{aligned} \tag{41}$$

However, the variation of the delay propagation error (e.g., generally at 10^{-8} s level) is much smaller than the one of the noise. Thus, the covariance term should be also much smaller than the variance of the noise. Consequently,

$$\sigma_{\delta\Im(\nu)},\quad \sigma_{\delta\Re(\nu)} \ll \sigma_{\Re(\nu)}^2$$

In addition, we also have

$$(\pi\,\Delta p\Delta f)^2 \gg 2\pi\,\Delta p\Delta f,$$

and the variance in (41) can be approximated by

$$\begin{aligned}\sigma_\Phi^2 &\approx (\pi\,\Delta p\Delta f)^2\sigma_\delta^2 + \frac{\sin^2(\theta)}{\alpha^2}\sigma_{\Re(\nu)}^2 + \frac{\cos^2(\theta)}{\alpha^2}\sigma_{\Im(\nu)}^2\\ &= (\pi\,\Delta p\Delta f)^2\sigma_\delta^2 + \sigma_n^2/N_p\alpha^2\end{aligned} \tag{42}$$

In order to further simplify (42), we first define the signal-to-noise ratio (SNR) of the LoS component. Considering a noise power in the time domain of $2\sigma^2$, which can be transformed to the frequency domain based on Parseval's theorem, the SNR can be written as

$$\begin{aligned}\mathrm{SNR}_{\mathrm{LoS}} &= \frac{\frac{1}{N}\sum_n |r_{bb}[n]|^2}{2\sigma^2} = \frac{\frac{1}{NN_p}\sum_k |R_k|^2}{2\sigma^2} \\ &= \frac{\frac{1}{N_p}\sum_k |R_k|^2}{2N\sigma^2} = \frac{\frac{1}{N_p}\sum_k |R_k|^2}{2\sigma_n^2},\end{aligned} \tag{43}$$

where R_k denotes the phasor of the received LoS component of the k-th subcarrier in the frequency domain. Considering the gain α of the LoS component, and assuming that all subcarriers are modulated for instance by BPSK (i.e., $|R_k| = \alpha|c_k| = \alpha$), then equation (43) can be written as

$$\mathrm{SNR}_{\mathrm{LoS}} = \frac{\alpha^2}{2\sigma_n^2}. \tag{44}$$

Since $|P_{\underline{\gamma}}^{\perp}\underline{\nu}|/|\underline{\gamma}|$ in (39) can be simplified as a Gaussian distributed variable, the estimated carrier phase approximately satisfies a Gaussian distribution (c.f. Appendix B) described as follows

$$\begin{aligned}&\underline{\Phi} \overset{a}{\sim} \mathcal{N}((-2\pi f_c\tau_1 \mod (-\pi,\pi]) - \pi\Delta p\Delta f\delta,\ \sigma_\Phi^2); \\ &\sigma_\Phi^2 \approx \pi^2\Delta p^2\Delta f^2\sigma_\delta^2 + \frac{1}{2N_p\mathrm{SNR}_{\mathrm{LoS}}}.\end{aligned} \tag{45}$$

We notice that even though there is a bias δ in the design matrix (30), its impact on the carrier phase estimate is relatively limited. For example, $\delta = 2\times10^{-8}$ s (converted into a distance of about 6 m) only causes a bias of 0.009 rad in the carrier phase estimate, when there are $N_P = N = 64$ pilot subcarriers with $\Delta p = 1$ in a 10 MHz bandwidth. For example, in an IEEE 802.11p based system with a central carrier frequency of 5.9 GHz (i.e., its wavelength is about 0.05 m), the phase bias due to the time delay error can be converted into 4.9×10^{-4} m of distance.

In addition, with increasing power of the noise σ_n^2, the performance of carrier phase estimation will be dominated by the noise instead of the time delay estimation error. Thus, we can have the following approximation

$$\sigma_\Phi^2 \approx \frac{1}{2N_p\mathrm{SNR}_{\mathrm{LoS}}} \tag{46}$$

IV. CARRIER PHASE-BASED POSITIONING MODEL

Since the carrier phase estimates are ambiguous as shown in (45), the geometry information can not be directly obtained from a single estimate. Therefore, in this section, we present a generic approach to compute positioning solutions only using the central carrier phase estimated from multiple time epochs.

A. PHASE AMBIGUITY

In the previous section, we proposed to estimate the central carrier phase, based on the time delay determined by the ESPRIT method, and evaluated its performance. However, the carrier phase estimated from (35) is always from $-\pi$ to π, which thus introduces an ambiguity. In addition, if the bias in the carrier phase estimate introduced by the time delay estimation error is negligible, the carrier phase can be approximated as

$$\begin{aligned}\underline{\Phi} &\approx (-2\pi f_c\tau_1 \mod (-\pi,\pi]) + \frac{|P_{\underline{\gamma}}^{\perp}\underline{\nu}|}{|\underline{\gamma}|} \\ &\approx (-2\pi f_c\tau_1 \mod (-\pi,\pi]) + \underline{e},\end{aligned} \tag{47}$$

where $\underline{e}$ denotes the Gaussian noise component with the variance shown in (45).

Due to the motion of the receiver, the carrier phase is time variant in practice. Considering a time invariant initial phase offset φ_0 as shown in (1), we can rewrite (47), with a discrete symbol index l,

$$\begin{aligned}\underline{\Phi}_l &\approx \big(-2\pi(f_c\tau_1' + f_{D,c,l}(N_g + N/2)T_s \\ &\quad + \phi_{D,c,l-1}) - \varphi_0\big) \mod (-\pi,+\pi] + \underline{e}_l \\ &= -2\pi f_c\frac{r_l}{c} - \varphi_0 + 2\pi M_l + \underline{e}_l,\end{aligned} \tag{48}$$

where

$$\begin{aligned}\Phi_l &= \mathrm{frac}\left\{-2\pi f_c\frac{r_l}{c} - \varphi_0\right\}, \\ -2\pi M_l &= \mathrm{int}\left\{-2\pi f_c\frac{r_l}{c} - \varphi_0\right\},\end{aligned}$$

Φ_l denotes the *fractional* part of the actual carrier phase and M_l denotes the unknown *integer* phase cycle ambiguity, r_l denotes the geometric distance between the transmitter and receiver during the l-th symbol, and c denotes the speed of light.

In fact, the initially unknown carrier phase offset φ_0 cannot be separated from the integer phase ambiguity M_l in (48). Without using the double-difference technique as in GNSS [31], or calibrating this initial phase offset, one is unable to retrieve the phase ambiguity as an integer value. Instead, we only estimate the phase ambiguity $M_{f,l}$ as a float/real number, and the observation model (48) is rewritten as

$$\begin{aligned}\underline{\Phi}_l &\approx -2\pi f_c\frac{r_l}{c} + 2\pi M_{f,l} + \underline{e}_l, \\ M_{f,l} &= M_l - \frac{\varphi_0}{2\pi}.\end{aligned} \tag{49}$$

Fig. 3 illustrates the relation among integer phase ambiguity M_l, float phase ambiguity $M_{f,l}$, the initial phase offset φ_0 and the wrapped phase measurements Φ_l.

B. PHASE UNWRAPPING

In a non-static positioning scenario, the unknown phase ambiguity M_l or $M_{f,l}$ can be time variant (i.e., depends on l). Consequently, it will lead to a rank defect in the positioning model because of too many unknown parameters, which will be introduced in the following subsection. Alternatively, we only preserve one *initial* time-invariant integer carrier phase ambiguity in the observation model, and absorb the change of the carrier phase cycle because of the movement

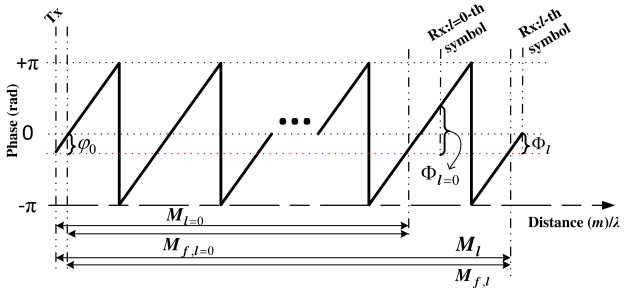

FIGURE 3. Phase ambiguities and wrapped phase estimates, in which the horizontal direction indicates the propagation distance in terms of wavelength of the central carrier frequency λ. $\Phi_{l=0}$ indicates the carrier phase estimate at the first epoch, which is ambiguous and contains only the fractional part of the physical carrier phase. Φ_l denotes the ambiguous carrier phase estimate from the l-th symbol. $M_{f,l}$ and M_l indicate the float and integer carrier phase cycle ambiguity, respectively.

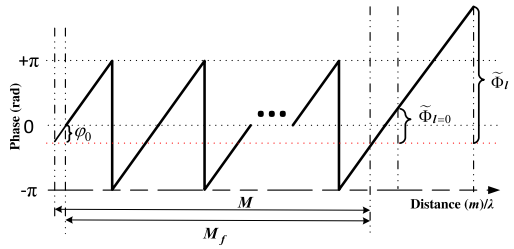

FIGURE 4. Phase ambiguities and unwrapped phase $\tilde{\Phi}$, in which only the initial phase ambiguity M (or M_f) is preserved.

of the receiver into the observations, namely by unwrapping a sequence of carrier phase estimates. This can be achieved by detecting phase jumps. When the phase estimation error is relatively small, we can simply compute differences between consecutive phase estimates and compare with a phase jump threshold, and determine whether a jump has occurred or not. Alternatively, the jump of the carrier phase cycle due to a change of positioning geometry can be estimated based on the integer least-squares estimation method [32]. Afterwards, the unwrapped phase estimate in the l-th OFDM symbol can be derived from (49) and be given as follows

$$\begin{aligned}\underline{\widetilde{\Phi}}_l &\approx -2\pi f_c \frac{r_l}{c} + 2\pi M - \varphi_0 + \underline{e}_l \\ &= -2\pi f_c \frac{r_l}{c} + 2\pi M_f + \underline{e}_l, \end{aligned} \tag{50}$$

where $\underline{\widetilde{\Phi}}$ denotes the unwrapped carrier phase estimate from (48). Thus, the symbol index l is removed from the unknown phase ambiguity in (50). M and M_f denote a time-invariant initial integer carrier phase ambiguity, and a time-invariant initial float carrier phase ambiguity, respectively. Similarly, the relation among the initial integer phase ambiguity M, the float ambiguity M_f, the initial phase offset φ_0 and unwrapped carrier phase estimates $\tilde{\Phi}$ is illustrated in Fig.4.

C. POSITIONING MODEL

In order to compute position solutions, we have to estimate the carrier phase from multiple transmitters. However, within a single epoch of observations, the phase estimate from each transmitter carries its own unknown ambiguity, and one is unable to obtain a unique position solution. Therefore, we also need to stack a series of unwrapped carrier phase estimates, in which the unknown initial carrier phase ambiguities are constant over the observation period.

In general, let the unwrapped carrier phase estimate of the l-th symbol belong to the time epoch t_l. Then, the positioning model based on m transmitters can be given as follows,

$$\begin{aligned}
\underline{\widetilde{\Phi}}^1(t_1) &= -2\pi f_c r_1(t_1)/c + 2\pi M_f^1 + \underline{e}^1(t_1) \\
\underline{\widetilde{\Phi}}^2(t_1) &= -2\pi f_c r_2(t_1)/c + 2\pi M_f^2 + \underline{e}^2(t_1) \\
&\vdots \\
\underline{\widetilde{\Phi}}^m(t_1) &= -2\pi f_c r_m(t_1)/c + 2\pi M_f^m + \underline{e}^m(t_1) \\
\underline{\widetilde{\Phi}}^1(t_2) &= -2\pi f_c r_1(t_2)/c + 2\pi M_f^1 + \underline{e}^1(t_2) \\
\underline{\widetilde{\Phi}}^2(t_2) &= -2\pi f_c r_2(t_2)/c + 2\pi M_f^2 + \underline{e}^2(t_2) \\
&\vdots \\
\underline{\widetilde{\Phi}}^m(t_2) &= -2\pi f_c r_m(t_2)/c + 2\pi M_f^m + \underline{e}^m(t_2) \\
&\vdots \\
\underline{\widetilde{\Phi}}^1(t_l) &= -2\pi f_c r_1(t_l)/c + 2\pi M_f^1 + \underline{e}^1(t_m) \\
\underline{\widetilde{\Phi}}^2(t_l) &= -2\pi f_c r_2(t_l)/c + 2\pi M_f^2 + \underline{e}^2(t_m) \\
&\vdots \\
\underline{\widetilde{\Phi}}^m(t_l) &= -2\pi f_c r_m(t_l)/c + 2\pi M_f^m + \underline{e}^m(t_m),
\end{aligned} \tag{51}$$

where $\underline{\widetilde{\Phi}}^m(t_l)$ denotes the unwrapped carrier phase estimate from the m-th transmitter at time epoch t_l, M_f^m denotes the unknown initial float carrier phase ambiguity for the m-th transmitter. In a 2D positioning geometry, solving the positioning model (51) requires at least $m = 4$ transmitters and $l = 2$ time epochs. The positioning geometry should change over these two observation epochs (i.e., the receiver should move), otherwise, it is still impossible to compute position solutions due to a matrix rank defect as we will see with (54), as shown at the bottom of the next page.

Given a fixed bandwidth, all transmitters can transmit ranging signals in time division multiplexing (TDM) to avoid interference. Alternatively, considering time efficiency, by means of orthogonal frequency division multiplexing access (OFDMA), each transmitter can occupy orthogonalized N_p comb-type pilots with a spacing of $\Delta p \Delta f$ as shown in Fig. 5. So the signal spectra for the transmitters are orthogonal. Furthermore, in small positioning area (e.g., 300 m × 300 m), the signal from different transmitters will not experience a significant difference on the propagation time delay (e.g., less than 1 μs). The transmitters can periodically transmit pilot signals for positioning within a certain time interval. In this paper, we focus on carrier phase based positioning with OFDM signals, an efficient embedding in an OFDM communication signal is subject to further research.

For the ease of notation, here we consider the minimum requirement to solve positioning model (51). Thus, using

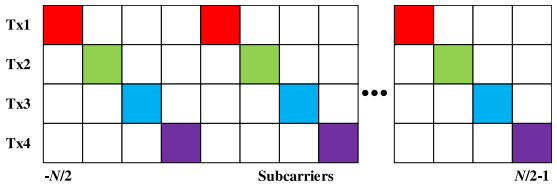

FIGURE 5. Frequency division multiplexing for multiple transmitters; different transmitters occupy different pilot subcarriers along the horizontal axis (in the example use $\Delta p = 4$).

phase estimates at two time epochs t_1 and t_2 from four transmitters. In a 2D positioning scenario, the geometric distance between the m-th transmitter and the receiver at time t_1 is

$$r_m(t_1) = \sqrt{(x_m - a(t_1))^2 - (y_m - b(t_1))^2}, \tag{52}$$

where x_m and y_m denote the known coordinates of the m-th transmitter, $a(\cdot)$ and $b(\cdot)$ denote the actual coordinates of the receiver at the indicated time.

Equation (51) presents a nonlinear least-squares estimation problem, which can be solved, for instance, by the Gauss-Newton iteration method [30]. Applying a Taylor series expansion to (52) and ignoring the higher order terms, the positioning model (51) can be rewritten in the following form

$$\underline{\boldsymbol{y}} = A_p \boldsymbol{x} + \underline{\boldsymbol{e}}. \tag{53}$$

As we can see, in a static scenario or if the positioning geometry does not experience a significant change over the observation period, the design matrix (54) will be rank defect or ill-conditioned. Therefore, positioning only based on the carrier phase estimates requires a change of geometry.

The unknown parameters in vector $\boldsymbol{x}$ and the measurements in vector $\underline{\boldsymbol{y}}$ in (53) can be respectively described as

$$\boldsymbol{x} = \begin{bmatrix} a(t_1) - a^0(t_1) & b(t_1) - a^0(t_1) & a(t_2) - a^0(t_2) \\ & b(t_2) - b^0(t_2) & M_f^1 & M_f^2 & M_f^3 & M_f^4 \end{bmatrix}^{\mathrm{T}},$$

$$\underline{\boldsymbol{y}} = \begin{bmatrix} \underline{\widetilde{\Phi}}^1(t_1) & \underline{\widetilde{\Phi}}^2(t_1) & \underline{\widetilde{\Phi}}^3(t_1) & \underline{\widetilde{\Phi}}^4(t_1) \\ & \underline{\widetilde{\Phi}}^1(t_2) & \underline{\widetilde{\Phi}}^2(t_2) & \underline{\widetilde{\Phi}}^3(t_2) & \underline{\widetilde{\Phi}}^4(t_2) \end{bmatrix}^{\mathrm{T}},$$

in which $a^0(\cdot)$ and $b^0(\cdot)$ denote the initial value (or iteratively updated value) of the unknown coordinates of the receiver.

The variance of the phase estimate can be derived from the signal model. Based on (45), for a sufficiently large SNR and in a moderate multipath condition (e.g., no strong close-in multipath), the carrier phase estimate approximately satisfies the following distribution

$$\underline{\widetilde{\Phi}}^m \overset{a}{\sim} \mathcal{N}\left(\widetilde{\Phi}^m, \underbrace{(\pi \Delta p \Delta f)^2 \sigma_\delta^2 + \frac{1}{2N_p \mathrm{SNR}_{\mathrm{LoS},m}}}_{\sigma^2_{\underline{\widetilde{\Phi}}^m}} \right). \tag{55}$$

where N_p stands for the number of pilots, $\mathrm{SNR}_{\mathrm{LoS},m}$ stands for the SNR of the LoS component for the m-th transmitter.

Based on the linearized observation model, we can solve (53) via the BLUE method [30], and the unknown estimators can be obtained from

$$\underline{\hat{\boldsymbol{x}}} = (A_p^{\mathrm{T}} Q_{\underline{\boldsymbol{y}}\underline{\boldsymbol{y}}}^{-1} A_p)^{-1} A_p^{\mathrm{T}} Q_{\underline{\boldsymbol{y}}\underline{\boldsymbol{y}}}^{-1} \underline{\boldsymbol{y}}, \tag{56}$$

where

$$Q_{\underline{\boldsymbol{y}}\underline{\boldsymbol{y}}} = \mathrm{diag}\left(\left[\sigma^2_{\underline{\widetilde{\Phi}}^1}, \ \sigma^2_{\underline{\widetilde{\Phi}}^2}, \ \sigma^2_{\underline{\widetilde{\Phi}}^3}, \ \sigma^2_{\underline{\widetilde{\Phi}}^4}, \ \sigma^2_{\underline{\widetilde{\Phi}}^1}, \ \ldots, \sigma^2_{\underline{\widetilde{\Phi}}^4} \right] \right).$$

The variance matrix of the least-squares solution can be derived from

$$Q_{\hat{\boldsymbol{x}}\hat{\boldsymbol{x}}} = \left(A_p^{\mathrm{T}} Q_{\underline{\boldsymbol{y}}\underline{\boldsymbol{y}}}^{-1} A_p \right)^{-1}.$$

V. SIMULATION RESULTS

The performance of the proposed carrier phase estimation method is evaluated in an OFDM-based system with a 10 MHz bandwidth, $N = 64$ subcarriers and $N_g = 16$

$$A_p = -2\pi \begin{bmatrix} f_c \frac{-(x_1 - a^0(t_1))}{cr_1(t_1)} & f_c \frac{-(y_1 - b^0(t_1))}{cr_1(t_1)} & 0 & 0 & -1 & 0 & 0 & 0 \\ f_c \frac{-(x_2 - a^0(t_1))}{cr_2(t_1)} & f_c \frac{-(y_2 - b^0(t_1))}{cr_2(t_1)} & 0 & 0 & 0 & -1 & 0 & 0 \\ f_c \frac{-(x_3 - a^0(t_1))}{cr_3(t_1)} & f_c \frac{-(y_3 - b^0(t_1))}{cr_3(t_1)} & 0 & 0 & 0 & 0 & -1 & 0 \\ f_c \frac{-(x_4 - a^0(t_1))}{cr_4(t_1)} & f_c \frac{-(y_4 - b^0(t_1))}{cr_4(t_1)} & 0 & 0 & 0 & 0 & 0 & -1 \\ 0 & 0 & f_c \frac{-(x_1 - a^0(t_2))}{cr_1(t_2)} & f_c \frac{-(y_1 - b^0(t_2))}{cr_1(t_2)} & -1 & 0 & 0 & 0 \\ 0 & 0 & f_c \frac{-(x_2 - a^0(t_2))}{cr_2(t_2)} & f_c \frac{-(y_2 - b^0(t_2))}{cr_2(t_2)} & 0 & -1 & 0 & 0 \\ 0 & 0 & f_c \frac{-(x_3 - a^0(t_2))}{cr_3(t_2)} & f_c \frac{-(y_3 - b^0(t_2))}{cr_3(t_2)} & 0 & 0 & -1 & 0 \\ 0 & 0 & f_c \frac{-(x_4 - a^0(t_2))}{r_4(t_2)} & f_c \frac{-(y_4 - b^0(t_2))}{cr_4(t_2)} & 0 & 0 & 0 & -1 \end{bmatrix}. \tag{54}$$

samples of CP. First we evaluate the performance of carrier phase estimation in multipath conditions. Afterwards, in a positioning system containing four transmitters, comb-type pilots are used in each transmitters to compute positioning solutions. In addition, the positioning scenario used in the following simulation is based on Fig. 1.

A. NOISE ANALYSIS: SINGLE-PATH CHANNEL

Since the central carrier phase is estimated based on the delay of the LoS path, we first analyze the impact of the time delay error on carrier phase estimation. Thus, we simulate the channel frequency response $\underline{\boldsymbol{H}}$ shown in (31) with only a LoS path, the performance for a multipath condition will be provided in the following sub-sections.

In a LoS path channel, the observations in (31) are only perturbed by the complex random noise $\underline{\boldsymbol{n}}$. Instead of computing the propagation delay, we simply generate a zero-mean time delay estimation error $\underline{\delta}$ with a fixed standard deviation σ_δ for every OFDM symbol, no matter the SNR. So that the design matrix for the carrier phase estimation in (26) can be constructed by $\mathbf{a}(\tau_1, \underline{\delta})$ shown in (30).

We choose three different noise levels (i.e., SNR $=$ 20, 10 and 0 dB) to evaluate the impact of the time delay error on carrier phase estimation. The signal bandwidth is assumed to be 10 MHz, thus the sampling interval T_s is 1×10^{-7} s. Fig. 6 (a) and (b) show the standard deviation of the carrier phase (on logarithmic scale) as a function of the standard deviation of the time delay error σ_δ for each SNR, when 16 pilots ($\Delta p = 4$) and all subcarriers ($\Delta p = 1$) are used for carrier phase estimation, respectively. Both the theoretical standard deviation as derived from (45), the approximation (46) and the empirical standard deviation computed from the simulation data (i.e., 10^6 OFDM symbols) are presented.

According to Fig. 6, using more pilot subcarriers for carrier phase estimation improves its accuracy. When the standard deviation of the time delay estimation error σ_δ is less than $0.2T_s$ (i.e., 6 m in distance), the derived standard deviation is generally in line with the empirical standard deviation. Especially, with a relatively low SNR (e.g., SNR $=$ 10 dB or smaller), the phase error is generally close to the square root of the variance approximated in (46). For a high SNR (e.g., SNR $=$ 20 dB), the approximated standard deviation deviates from the empirical standard deviation, because the phase error is dominated by the error of time delay shown in (45). The results start to deviate when the time delay error increases (e.g., $\sigma_\delta > 0.2T_s$), which is mainly because the approximations used in (33) and (36) are no longer valid, and the random time delay error should be taken into account.

Now, let the propagation delay be determined by the ESPRIT method based on the channel measurements, and then estimate the carrier phase. Fig. 7(a) shows the empirical standard deviation of the ESPRIT-based time delay estimation error as a function of SNR. Since the standard deviation of the time delay error is far less than $0.2T_s$, the carrier phase estimation error is dominated by the noise. In Fig. 7(b),

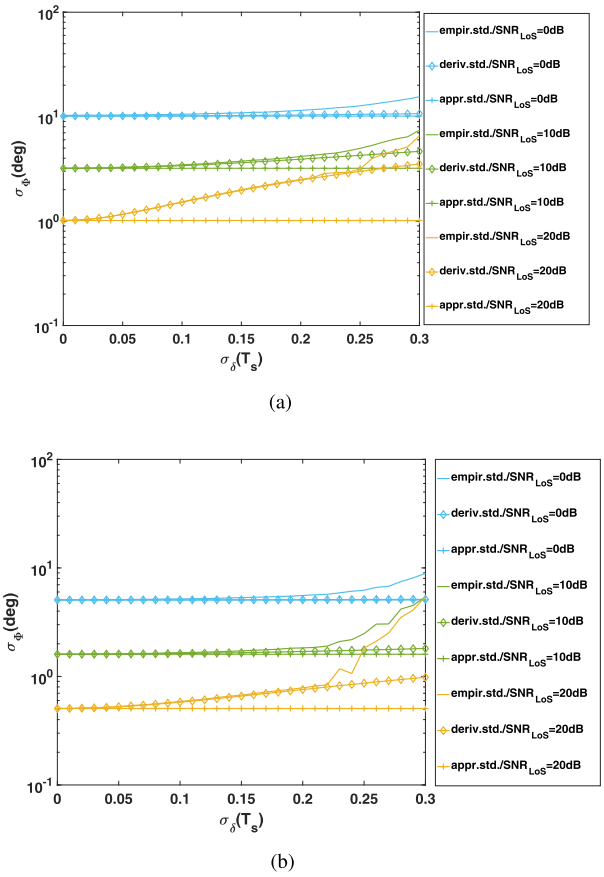

FIGURE 6. (a) Using only $N_p = 16$ pilot subcarriers with a spacing of $\Delta p = 4$ and (b) using all subcarriers $N = N_p = 64$ with a spacing of $\Delta p = 1$ (b), standard deviation of carrier phase estimation error σ_Φ versus standard deviation of time delay error σ_δ (in units of T_s) for three different SNRs 0, 10, and 20 dB, in which 'empir.std.' denotes the empirical standard deviation computed from the simulation, 'eriv.std.' denotes the theoretical standard deviation derived from (45), and 'appr.std.' denotes the approximation of the standard deviation in (46).

the empirical standard deviation of the observed carrier phase is well in line with the derived standard deviation (46).

In order to validate the assumption of the distribution of the estimators, Fig. 8 presents a histogram of the time delay error and the carrier phase error from 6×10^4 OFDM symbols. In Fig. 8(a), the distribution of the time delay error looks close to a Gaussian shape, and therefore we approximate it as a Gaussian distribution. In fact, since the variance of the time delay error is much smaller than that of the thermal noise, its impact on carrier phase estimation can be even neglected. Consequently, the carrier phase error, which is mainly dominated by the Gaussian thermal noise, will satisfy a Gaussian distribution as well and is shown in Fig. 8(b).

The propagation delay determined by the ESPRIT method can achieve a (deci-)meter level accuracy in a single path channel. Based on this time delay, the LoS carrier phase is accurately estimated in the second step. Although the phase ambiguity problem is introduced, the phase provides a much higher time resolution than time delay estimation. For example, considering a 5.9 GHz central frequency, a 5 degree phase uncertainty only causes 0.07 cm of uncertainty in distance.

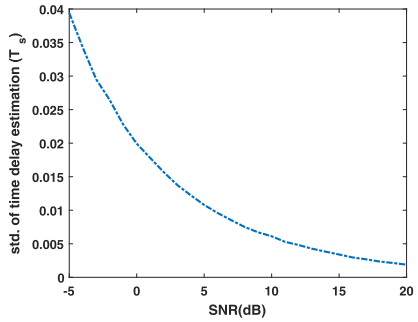

(a)

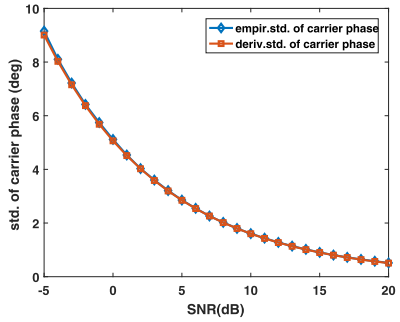

(b)

FIGURE 7. (a) Empirical standard deviation of time delay σ_δ and (b) both the empirical and derived standard derivation σ_Φ (46) of carrier phase estimation versus SNR.

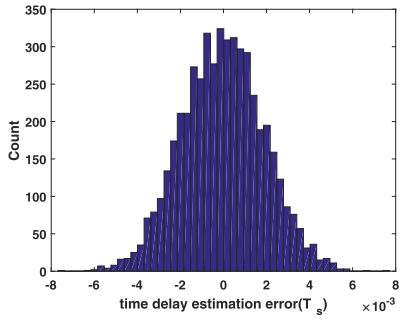

(a)

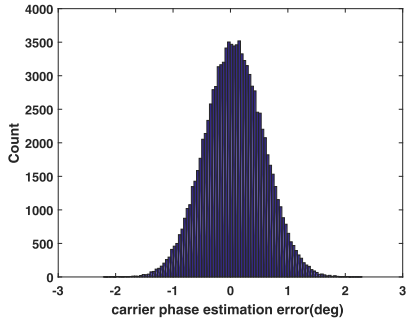

(b)

FIGURE 8. (a) histogram of ESPRIT-based time delay error as SNR = 20dB, (b) histogram of carrier phase estimation error as SNR = 20dB.

B. NOISE ANALYSIS: MULTIPATH CHANNELS

Before we evaluate the performance of carrier phase estimation based on the proposed two-step approach, we investigate

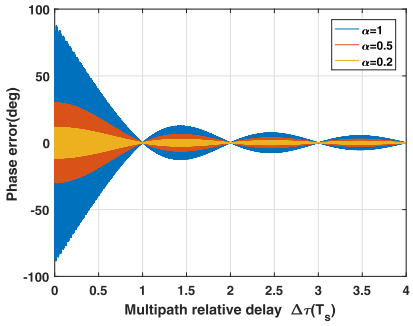

FIGURE 9. Envelope of additional multipath carrier phase error for different relative gains, in which as a function of relative delay $\Delta\tau = \tau_2 - \tau_1$.

TABLE 1. Tapped-delay-line parameters for vehicular test environment.

Channel	Tap	time delays (ns)	average power (dB)
Vehicular A	1	0	0
	2	310	-1
	3	710	-9
	4	1090	-10
Highway Los	1	0	0
	2	100	-10
	3	167	-15
	4	500	-20

the characteristics of the additional multipath phase error based on (26) in a two-path channel (i.e., direct LoS and one reflection, $P = 2$). Given a static receiver and a static channel, the additional phase error is deterministic and constant. However, the additional phase error becomes arbitrary in a non-static positioning scenario. In fact, it is not straightforward to derive its PDF. Thus in Fig. 9 we only illustrate the envelope of the additional phase error considering a single reflection with different relative delays $\Delta\tau$ and relative gain α of the reflection.

A relatively strong reflection with a small relative delay can cause a considerable additional multipath phase error, which is jointly determined by the relative gain α and the term $|T(\Delta\tau)|$ defined in (25). Then, the covariance matrix (24) cannot be simply assumed to be a diagonal matrix. However, reflections tend to be well separated from the LoS path in an outdoor environment, for example in a roadway/highway scenario. In such a condition, using the proposed approach, the impact of multipath on carrier phase estimation can be significantly reduced.

Two different outdoor multipath models shown in Table 1 are introduced to evaluate the proposed two step carrier phase estimation method. Since we assume that the receiver shown in Figure 1 is moving with a constant speed of 80 km/h, the maximum Doppler shift of the channel is about 437 Hz, for a carrier frequency of 5.9 GHz.

In the 'Vehicular A' channel [33], since the relative delays of all reflections are larger than one sample interval T_s, all paths can be assumed to be sufficiently well separable.

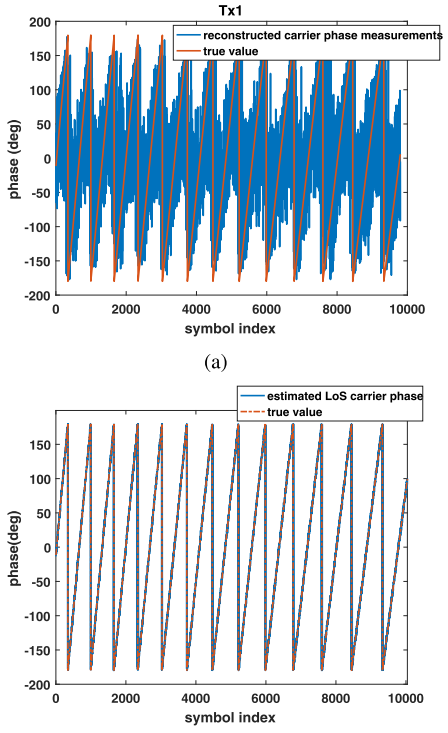

FIGURE 10. 'Vehicular A' multipath channel with SNR = 20 dB, (a) carrier phase derived based on phase combination of two symmetrically located subcarriers (e.g., (+/−12)-th subcarrier) [34]; (b) LoS carrier phase estimated from proposed two-step approach.

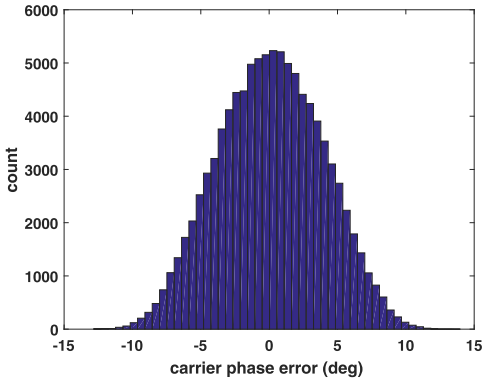

FIGURE 11. Histogram of LoS carrier phase error (σ_ϕ = 4.78 degree), when SNR_{LoS} = 20dB in the 'Vehicular A' multipath channel.

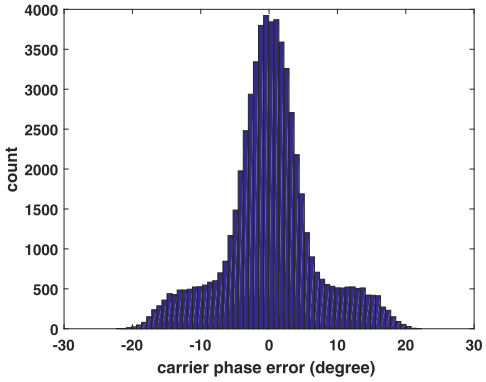

FIGURE 12. Histogram of carrier phase error estimated from proposed method in the 'Highway LoS' channel. Because of the large additional multipath phase error, the distribution of the carrier phase error will no longer have a Gaussian shape.

In such a case, the carrier phase can be estimated by means of the proposed two-step method. Here we use all subcarriers as pilots for time delay estimation and carrier phase estimation. For comparison, we also derive the central carrier phase (i.e., from the zero-subcarrier) by combining the phase from two symmetrically located pilot subcarriers (e.g., the (-12)-th and the 12-th subcarrier) [34]. The carrier phase derived based on the phase combination from two symmetrically located subcarriers is shown Fig. 10(a), and we can notice that the carrier phase directly obtained from the combination is largely perturbed by multipath, especially when the reflections have relatively large power.

Alternatively, using the proposed two-step LoS carrier phase estimation approach, the impact of multipath on phase estimation, as shown in Fig. 10(b), is significantly mitigated.

Fig. 11 shows a histogram of the phase error. When SNR_{LoS} = 20 dB, the standard deviation of the carrier phase is σ_Φ = 4.78 degree, which is different from the value presented in Fig. 7. The increase is mainly because of the additional multipath phase error. For example, in the 'Vehicular A' channel, the second path can still cause about 2 degree of additional phase error. This additional multipath error is smaller than the one from thermal noise. In such a condition, the resulting phase estimation error shown in Fig. 11 still approximately looks like a Gaussian distribution.

On the other hand, in the 'Highway LoS' channel [19], although the average power of the reflections are smaller than the ones in the 'Vehicular A' channel, the relative delays are also much smaller and close to $1T_s$. According to Fig. 9, the additional multipath phase error could be larger than the multipath phase error in the 'Vehicular A' channel. Similarly, Fig. 12 shows the histogram of the carrier phase error when SNR_{LoS} = 20 dB. Since the additional multipath error disperses over an interval that can be even wider than the one caused by the Gaussian thermal noise, the distribution of the carrier phase error will no longer be Gaussian. The standard deviation of the carrier phase error σ_Φ is about 6.55 degrees and larger than the value derived from (45).

C. POSITIONING RESULTS

The performance of carrier phase estimation has been analyzed in the previous sections. In order to compute the position solution, we let all transmitters and the receiver be synchronized to the same time and frequency source, and different transmitters occupy different pilots in the given bandwidth, as shown in Fig. 5. Thus, the spectra for all transmitters are orthogonal, and each transmitter uses 16 comb-type pilots (Δp = 4) for ranging. Based on the proposed approach, the unwrapped carrier phase estimates for the signals from four transmitters in the 'Vehicular A' channel are shown in Fig. 13, when the SNR_{LoS} is 20dB.

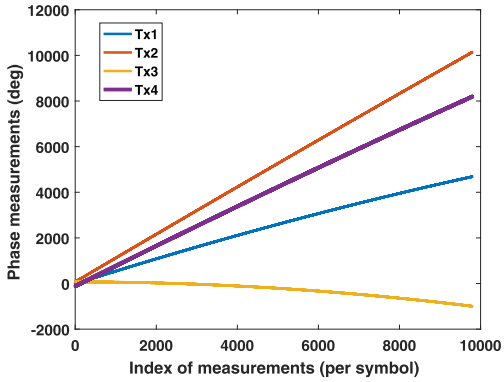

FIGURE 13. Considering the positioning scenario shown in Fig. 1 and the 'Vehicular A' channel, unwrapped LoS carrier phase measurements on signals from four transmitters.

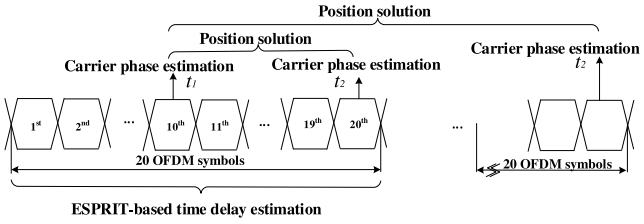

FIGURE 14. Time delay estimation and carrier phase estimation from OFDM symbols. t_1 is kept to the 10-th symbol and t_2 is updated every next 10-th symbol.

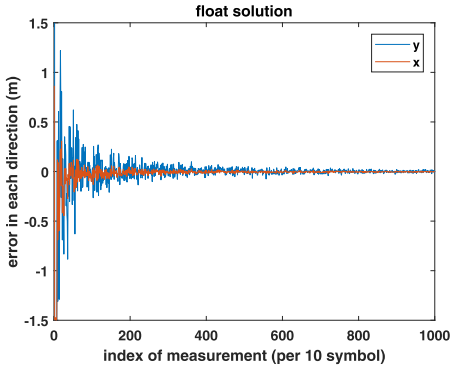

FIGURE 15. Error of float position solution in x and y direction, when SNR = 20 dB (c.f. Fig. 1).

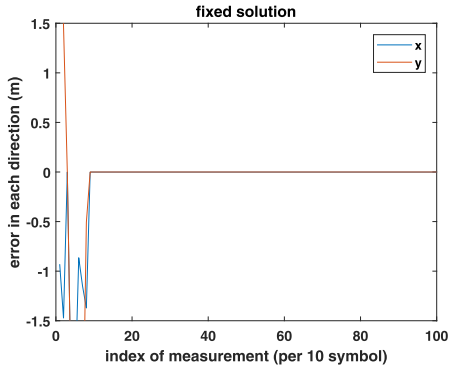

FIGURE 16. Error of fixed position solution along the x and y direction, when SNR = 20dB.

Now, the position solution is computed based on the unwrapped carrier phase measurements, and each time we only use the measurements from two epochs. For each transmitter, 10^5 OFDM symbols are generated for positioning. Although we can estimate the carrier phase in every OFDM symbol, the transmitter-receiver geometry does not change significantly over a few number of OFDM symbols. For example, considering the positioning scenario in Fig. 1, we first compute the propagation delay based on the ESPRIT method over every 20 OFDM symbols. Depending on the velocity of the receiver, the geometry may not experience a significant change, thus it is not necessary to estimate the carrier phase in every OFDM symbol. As an example, we only estimate the carrier phase from every 10-th OFDM symbol. The estimation process can be conducted as shown in Fig. 14. In addition, positioning only based on the carrier phase requires the measurements from multiple time epochs. The measurement at the first epoch $t = t_1$ is always kept in (51), then we choose every next 10-th OFDM symbol for the second epoch $t = t_2$.

Due to the time-invariant initial phase offset φ_0 in (48), we do not fix the phase ambiguity as an integer number. Thus, only a *float* position solution can be obtained, which is shown in Fig. 15 as a function of time t_2. The carrier phase based position solution requires a change of the transmitter-receiver geometry as outlined in section IV-C. At the beginning, the Tx-Rx geometry at t_1 and t_2 is very similar and the design matrix A_p in (54) is poorly conditioned. We can observe from Fig. 15 that the positioning error converges after 5000 (i.e., 500×10) OFDM symbols (i.e., t_1 and t_2 are separated by 4×10^{-2} s). Therefore, the root-mean-square error (RMSE) of the float positioning solution is computed after the 500-th phase measurement. Then, the RMSE along the x-direction is 0.17 cm, and the RMSE along the y direction is 0.54 cm.

Even though an initial carrier phase offset is considered in (50), if the bias introduced by the time-invariant phase offset is negligible for the system or can be accepted by users, we can still fix the phase ambiguity into an integer number. Using the least-squares ambiguity de-correlation adjustment (LAMBDA) method [35] and its software package [36], developed for high precision GNSS positioning, the error of the fixed positioning solution is shown in Fig. 16. We can notice that the phase ambiguity can be fixed only after about 150 OFDM symbols (i.e., 1.2×10^{-3} s). In addition, when the carrier phase ambiguities can be properly fixed to integer numbers, the system requires less time of convergence, and the positioning error can be further reduced by at least one order of magnitude. In such a case, the RMSE along the x-direction is 5.9×10^{-2} cm and the RMSE along the y-direction is 2.8×10^{-2} cm.

So far we only assume a time invariant carrier phase offset, it is worth to mention here that if the phase offset becomes time variant due the sampling frequency offset, and causes cycle-slips in the observations, the unknown carrier phase ambiguity may not be constant over the observation period.

VI. CONCLUSION

In this paper, we investigate the possibility of precise positioning based on OFDM signals through carrier phase measurements in a time and frequency synchronized system. In order to mitigate the impact of multipath on carrier phase estimation, we propose a two-step estimation method. First, the propagation delay is coarsely determined. Then, the phase from the central carrier is estimated based on the propagation delay. Although using only carrier phase estimates introduces an ambiguity problem in positioning, it can provide a much higher time resolution and more precise geometric information than time delay measurements, as long as we can properly unwrap the carrier phase estimates.

Analysis and simulation results show that the carrier phase estimation error based on the proposed method seems to approximately have a Gaussian distribution when the standard deviation of the time delay error in the first step is less than 20 ns (i.e., about 6 m in distance). Considering an SNR of 20 dB, without fixing the phase ambiguities to integer numbers, the so-called float position solution already achieves sub-centimetre level accuracy. Based on the system setup shown in Fig. 1, a change of at least 0.9 m in distance is required to let the solution converge. In addition, if the system bias introduced by the time-invariant initial carrier phase offset is negligible or can be accepted by users, then the carrier phase ambiguities can be still fixed to integer numbers. Consequently, by fixing the ambiguities the convergence time will significantly decrease. Thus, given a relatively narrow signal bandwidth, carrier phase estimation based on the proposed method offers robust accurate positioning in the indicated multipath condition. Consequently, positioning based on carrier phase measurement is a promising approach to achieve high positioning accuracy. Future work will be conducted on an asynchronous system, in which the transmitters and the receiver will be no longer synchronized by the same clock. For instance, the sampling clock offset can result in a time-variant phase error in carrier phase estimation, and cause difficulties in phase unwrapping and fixing the phase ambiguity.

APPENDIX

A. PROOF OF (31)

Using comb-type pilots for carrier phase estimation, the signal has N_p pilots with a spacing of Δp. Based on the signal model shown in (26), the complex gain x can be computed based on the ordinary (un-weighted) least-squares estimation. Since

$$\boldsymbol{a}(\tau_1, \underline{\delta})^{\mathrm{H}} \boldsymbol{a}(\tau_1, \underline{\delta}) = N_p,$$

we can express $\hat{\underline{x}}$ as

$$\begin{aligned}\hat{\underline{x}} &= (\boldsymbol{a}(\tau_1, \underline{\delta})^{\mathrm{H}} \boldsymbol{a}(\tau_1, \underline{\delta}))^{-1} \boldsymbol{a}(\tau_1, \underline{\delta})^{\mathrm{H}} \underline{\boldsymbol{H}} \\ &= \frac{1}{N_p} \sum_{i=-N_p/2}^{N_p/2-1} \exp(j2\pi f_i(\tau_1 + \underline{\delta}))(H_i + \underline{n}_i) \\ &= \frac{\alpha}{N_p} \exp(-j2\pi f_c \tau_1) \exp\left(-j2\pi \frac{N_p}{2} \Delta p \Delta f \underline{\delta}\right) \\ &\quad \times \sum_{i=0}^{N_p-1} \exp(j2\pi i \Delta p \Delta f \underline{\delta}) \\ &\quad + \frac{1}{N_p} \sum_{i=-N_p/2}^{N_p/2-1} \exp\left(j2\pi i \Delta p \Delta f (\tau_1 + \underline{\delta})\right) \underline{n}_i. \end{aligned} \tag{57}$$

Using

$$\sum_{n=0}^{N-1} \exp(jnx) = \frac{\sin\left(\frac{1}{2}Nx\right)}{\sin\left(\frac{1}{2}x\right)} \exp\left(jx\frac{(N-1)}{2}\right),$$

(57) can be reduced to

$$\begin{aligned}\hat{\underline{x}} &= \frac{\alpha}{N_p} \exp(-j2\pi f_c \tau_1) \\ &\quad \times \exp\left(-j\pi \Delta p \Delta f \underline{\delta}\right) \frac{\sin\left(\frac{N_p}{2} 2\pi \Delta p \Delta f \underline{\delta}\right)}{\sin\left(\frac{1}{2} 2\pi \Delta p \Delta f \underline{\delta}\right)} \\ &\quad + \frac{1}{N_p} \sum_{i=-N_p/2}^{N_p/2-1} \exp(j2\pi i \Delta p \Delta f (\tau_1 + \underline{\delta})) \underline{n}_i. \end{aligned} \tag{58}$$

Then, combined with (25), (58) is further simplified to (31).

B. VALIDATION OF (32)

In order to validate the approximation of the two PDFs shown in (32), we first analyse the following equation

$$\underline{r}_k = \underline{n}_k \exp\left(j2\pi f_k(\tau_1 + \underline{\delta})\right), \tag{59}$$

where $\underline{n}_k$ denotes zero-mean Gaussian noise on the k-th subcarrier, $\underline{\delta}$ denotes the time delay error, which is assumed to be normally distributed. Furthermore, we assume $\underline{n}_k$ and $\underline{\delta}$ to be uncorrelated, and have the following distributions,

$$\begin{bmatrix} \Re\{\underline{n}_k\} \\ \Im\{\underline{n}_k\} \end{bmatrix} \sim \mathcal{N}\left(\begin{bmatrix} 0 \\ 0 \end{bmatrix}, \begin{bmatrix} \sigma_n^2 & 0 \\ 0 & \sigma_n^2 \end{bmatrix}\right), \quad \underline{\delta} \sim \mathcal{N}(\delta, \sigma_\delta^2).$$

Since $\underline{n}_k$ in (59) is a complex Gaussian variable, which can also be written as

$$\underline{n}_k = \underline{\rho} \exp(j\underline{\phi}), \tag{60}$$

where the phase $\underline{\phi}$ is uniformly distributed from $-\pi$ to π. Now equation (59) can be rewritten as

$$\underline{r}_k = \underline{\rho} \exp(j(\underline{\phi} + \underline{\varphi}_k)), \quad \underline{\varphi}_k = 2\pi f_k(\tau_1 + \underline{\delta}) \tag{61}$$

where $\underline{\varphi}_k$ stands for the phase rotation due to the propagation delay τ_1 and the time delay error $\underline{\delta}$. Thus, $\underline{\varphi}_k$ also satisfies a normal distribution given by,

$$\underline{\varphi}_k \sim \mathcal{N}\left(2\pi f_k(\tau_1 + \delta), 4\pi^2 f_k^2 \sigma_\delta^2\right)$$

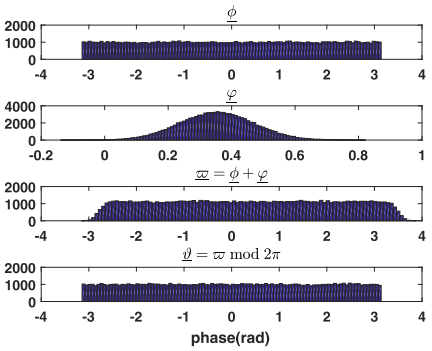

(a)

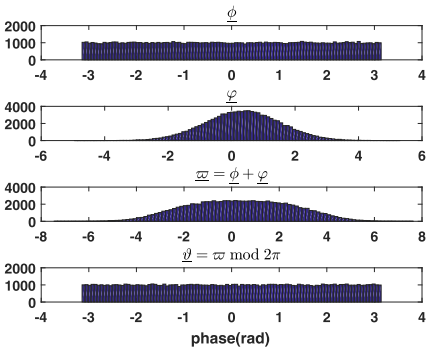

(b)

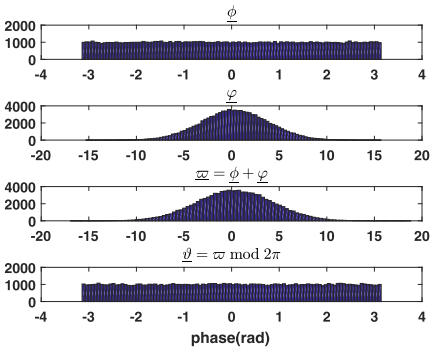

(c)

FIGURE 17. Histograms of the phase variables in (62), in which the vertical axis shows the occurrence in 10^4 times. The 12-th subcarrier is used in this simulation (i.e., $f_k = 12/NT_s$, $N = 64$, and $T_s = 10^{-7}$ s). Since $\underline{n_k}$ is complex Gaussian noise, $\underline{\phi}$ is uniformly distributed. (a) $\sigma_\delta = 0.1T_s$, (b) $\sigma_\delta = 1T_s$ and (b) $\sigma_\delta = 3T_s$. Since the unwrapped phase $\underline{\varpi}$ well spreads over the interval from $-\pi$ to π, the wrapped phase $\underline{\vartheta}$ still satisfies a uniform distribution.

Moreover, since the phase that can be estimated from $\underline{r}_k$ always varies from $-\pi$ to π, equation (61) can be written as

$$\begin{aligned} \underline{r}_k &= \underline{\rho} \exp(j\underline{\varpi}_k) = \underline{\rho} \exp(j\underline{\vartheta}_k) \\ \underline{\varpi}_k &= \underline{\phi} + \underline{\varphi}_k \\ \underline{\vartheta}_k &= \underline{\varpi}_k \mod (-\pi, \pi]. \end{aligned} \tag{62}$$

In order to analyze the phase $\underline{\varphi}_k$, we can first examine the phase without the unwrapped phase (i.e., $\underline{\varpi}_k$), which is a summation of a uniformly distributed variable and a Gaussian variable. In fact, it is difficult to derive the specific PDF for $\underline{\varpi}_k$, but we can still roughly determine its shape. If the distribution of $\underline{\varpi}_k$ has a wide spread, then the wrapped phase $\underline{\vartheta}_k$ tends toward a uniform distribution in the interval of $(-\pi, \pi]$.

Fig. 17 shows the histogram of the phase variables in (62) for different value of σ_δ. Because of the complex Gaussian noise, its phase $\underline{\phi}$ has a uniform distribution. When the standard deviation of the propagation delay is relatively small as in Fig 17(a), there will be a plateau in the histogram of the unwrapped phase $\underline{\varpi}$. Consequently, the wrapped phase $\underline{\vartheta}$ will still approximately satisfy a uniform distribution. On the other hand, with an increasing standard deviation of the time delay estimation $\underline{\delta}$ shown in Fig. 17(b) and (c), the distribution of $\underline{\varpi}$ is mainly dominated by the Gaussian distributed phase error $\underline{\phi}$ instead of the delay error $\underline{\varphi}$ (mind the different horizontal scales). In such a case, due to a relatively large standard deviation of $\underline{\varpi}$, its value can be well spread over the interval from -π to π. Therefore, the wrapped phase $\underline{\vartheta}$ can be still approximated by a uniform distribution.

Then, the PDF of $\underline{r}_k$ can be approximated by the PDF of the complex Gaussian noise $\underline{n}_k$ in (59). For the purpose of statistical analysis, it can equivalently be written as

$$\begin{aligned} \underline{r}_k &= \underline{n}_k \exp\left(j2\pi f_k(\tau_1 + \underline{\delta})\right) = \underline{\rho} \exp(j\underline{\varpi}_k) \\ &\sim \underline{\rho} \exp(j\underline{\phi}) = \underline{n}_k \end{aligned} \tag{63}$$

ACKNOWLEDGMENT

TU Delft Library is acknowledged for providing the Open Access Fund for publishing this manuscript.

REFERENCES

[1] R. Beard and K. Senior, "Clocks," in *Springer Handbook of Global Navigation Satellite Systems*, P. Teunissen and O. Montenbruck, Eds. New York, NY, USA: Springer, 2017, ch. 6.

[2] M. S. Braasch, "Multipath," in *Springer Handbook of Global Navigation Satellite Systems*, P. Teunissen and O. Montenbruck, Eds. New York, NY, USA: Springer, 2017, ch. 15.

[3] L. Chen, O. Julien, P. Thevenon, D. Serant, A. G. Pena, and H. Kuusniemi, "TOA estimation for positioning with DVB-T signals in outdoor static tests," *IEEE Trans. Broadcast.*, vol. 61, no. 4, pp. 625–638, Dec. 2015.

[4] L. Chen, P. Thevenon, G. Seco-Granados, O. Julien, and H. Kuusniemi, "Analysis on the TOA tracking with DVB-T signals for positioning," *IEEE Trans. Broadcast.*, vol. 62, no. 4, pp. 957–961, Dec. 2016.

[5] D. Vasisht, S. Kumar, and D. Katabi, "Decimeter-level localization with a single WiFi access point," in *Proc. NSDI*, vol. 16, 2016, pp. 165–178.

[6] J. Xiong, K. Sundaresan, and K. Jamieson, "Tonetrack: Leveraging frequency-agile radios for time-based indoor wireless localization," in *Proc. 21st Annu. Int. Conf. Mobile Comput. Netw.*, 2015, pp. 537–549.

[7] J. A. del Peral-Rosado, J. A. Lopez-Salcedo, G. Seco-Granados, F. Zanier, and M. Crisci, "Achievable localization accuracy of the positioning reference signal of 3GPP LTE," in *Proc. Int. Conf. Localization GNSS*, Jun. 2012, pp. 1–6.

[8] J. A. del Peral-Rosado, J. A. Lopez-Salcedo, F. Zanier, and G. Seco-Granados, "Position accuracy of joint time-delay and channel estimators in LTE networks," *IEEE Access*, vol. 6, pp. 25185–25199, 2018.

[9] J. A. del Peral-Rosado, J. A. Lopez-Salcedo, S. Kim, and G. Seco-Granados, "Feasibility study of 5G-based localization for assisted driving," in *Proc. Int. Conf. Localization GNSS (ICL-GNSS)*, Jun. 2016, pp. 1–6.

[10] A. Makki, A. Siddig, C. Bleakley, M. Saad, and J. Cavallaro, "High-resolution time of arrival estimation for OFDM-based transceivers," *Electron. Lett.*, vol. 51, no. 3, pp. 294–296, Feb. 2015.
[11] R. Roy and T. Kailath, "ESPRIT-estimation of signal parameters via rotational invariance techniques," *IEEE Trans. Acoust., Speech, Signal Process.*, vol. 37, no. 7, pp. 984–995, Jul. 1989.
[12] O. Simeone, Y. Bar-Ness, and U. Spagnolini, "Pilot-based channel estimation for OFDM systems by tracking the delay-subspace," *IEEE Trans. Wireless Commun.*, vol. 3, no. 1, pp. 315–325, Jan. 2004.
[13] B. Yang, K. Letaief, R. Cheng, and Z. Cao, "Channel estimation for OFDM transmission in multipath fading channels based on parametric channel modeling," *IEEE Trans. Commun.*, vol. 49, no. 3, pp. 467–479, Mar. 2001.
[14] V. U. Prabhu and D. Jalihal, "An improved ESPRIT based time-of-arrival estimation algorithm for vehicular OFDM systems," in *Proc. IEEE 69th Veh. Technol. Conf. (VTC-Spring)*, Apr. 2009, pp. 1–4.
[15] C. Yang, L. Chen, O. Julien, S. Andrey, and R. Chen, "Carrier phase tracking of OFDM-based DVB-T signals for precision ranging," in *Proc. 30th Int. Tech. Meeting The Satell. Division Inst. Navigat.*, 2017, pp–736.
[16] J. Khalife and Z. M. Kassas, "Precise UAV navigation with cellular carrier phase measurements," in *Proc. IEEE/ION Position, Location Navigat. Symp. (PLANS)*, Apr. 2018, pp. 978–989.
[17] K. Shamaei, J. Khalife, and Z. M. Kassas, "Exploiting LTE signals for navigation: Theory to implementation," *IEEE Trans. Wireless Commun.*, vol. 17, no. 4, pp. 2173–2189, Apr. 2018.
[18] K. Shamaei and Z. M. Kassas, "LTE receiver design and multipath analysis for navigation in urban environments," *Navigation*, vol. 65, no. 4, pp. 655–675, Dec. 2018.
[19] T. Blazek, M. Ashury, C. F. Mecklenbrauker, D. Smely, and G. Ghiaasi, "Vehicular channel models: A system level performance analysis of tapped delay line models," in *Proc. 15th Int. Conf. Telecommun. (ITST)*, May 2017, pp. 1–8.
[20] Y. Li, "Basic concepts," in *Orthogonal Frequency Division Multiplexing for Wireless Communications*, Y. Li and G. L. Stuber, Eds. New York, NY, USA: Springer, 2006, ch. 5.
[21] A. Goldsmith, "Statistical multipath channel models," in *Wireless Communications*. Cambridge, U.K.: Cambridge Univ. Press, 2005, ch. 3.
[22] ETSI Technical Committee, "Broadband radio access networks (BRAN); 5 GHz high performance RLAN; Mitigation techniques to enable sharing between RLANs and road tolling and intelligent transport systems in the 5 725 MHz to 5 925 MHz band," ETSI, Sophia Antipolis, France, Tech. Rep. 103 319, 2017.
[23] H. D. Young, R. A. Freedman, T. Sandin, and A. L. Ford, *University Physics*, vol. 9. Reading, MA, USA: Addison-Wesley, 1996.
[24] Y. Li and L. Cimini, "Bounds on the interchannel interference of OFDM in time-varying impairments," *IEEE Trans. Commun.*, vol. 49, no. 3, pp. 401–404, Mar. 2001.
[25] Y. Li, "Channel estimation," in *Orthogonal Frequency Division Multiplexing for Wireless Communications*, Y. Li and G. L. Stuber, Eds. New York, NY, USA: Springer, 2006, ch. 5.
[26] P. Stoica and R. L. Moses, *Introduction to Spectral Analysis*, vol. 1. Upper Saddle River, NJ, USA: Prentice-Hall, 1997.
[27] A.-J. Van Der Veen, E. Deprettere, and A. Swindlehurst, "Subspace-based signal analysis using singular value decomposition," *Proc. IEEE*, vol. 81, no. 9, pp. 1277–1308, Sep. 1993.
[28] G. Xu, R. H. Roy, and T. Kailath, "Detection of number of sources via exploitation of centro-symmetry property," *IEEE Trans. Signal Process.*, vol. 42, no. 1, pp. 102–112, Jan. 1994.
[29] S. M. Kay, *Fundamentals of Statistical Signal Processing*. Upper Saddle River, NJ, USA: Prentice-Hall, 1993.
[30] P. Teunissen, D. Simons, and C. Tiberius, *Probability and Observation Theory*. Delft, The Netherlands: Delft Univ. Technol., 2004.
[31] D. Odijk and L. Wanniger, "Differential positioning," in *Springer Handbook of Global Navigation Satellite Systems*, P. Teunissen and O. Montenbruck, Eds. New York, NY, USA: Springer, 2017, ch. 26.
[32] P. Teunissen, "On InSAR ambiguity resolution for deformation monitoring," *Artif. Satell.*, vol. 41, no. 1, pp. 19–22, 2006.
[33] ETSI SMG, "Overall requirements on the radio interface (s) of the UMTS," ETSI, Valbonne, France, Tech. Rep. ETR/SMG-21.02, 1997, vol. 3.
[34] H. Dun, C. C. J. M. Tiberius, and G. J. M. Janssen, "Positioning based on OFDM signals through phase measurements," in *Proc. Signal Workshop (NAVITEC)*, 2018.
[35] P. J. G. Teunissen, "The least-squares ambiguity decorrelation adjustment: A method for fast GPS integer ambiguity estimation," *J. Geodesy*, vol. 70, nos. 1–2, pp. 65–82, Nov. 1995.
[36] S. Verhagen, B. Li, and P. J. Teunissen, "LAMBDA software package MATLAB implementation, version 3.0," Dept. Geosci. Remote Sens., Delft Univ. Technol., GNSS Res. Centre, Curtin Univ., Perth, WA, Australia, 2012.

HAN DUN received the B.Sc. degree in communication engineering and the M.Sc. degree in communication and information engineering from Shanghai University, China, in 2013 and 2016, respectively. He is currently pursuing the Ph.D. degree with the Department of Geoscience and Remote Sensing, Delft University of Technology, The Netherlands. From 2013 to 2016, he was with the Key Laboratory of Specialty Fiber Optics and Optical Access Network, Shanghai University. His research interests include digital communication theory, wireless localization, and statistical signal processing.

CHRISTIAN C. J. M. TIBERIUS received the Ph.D. degree from the Delft University of Technology, Delft, The Netherlands, in 1998, on recursive data processing for kinematic GPS surveying. He is currently an Associate Professor with the Geoscience and Remote Sensing (GRS) Department, Delft University of Technology. His research interests include in navigation with GNSS and terrestrial radio systems in particular in high-precision and high-integrity positioning with assisted and automated driving of road vehicles as a target application.

GERARD J. M. JANSSEN received the M.Sc. degree in E.E. from the Eindhoven University of Technology, Eindhoven, The Netherlands, in 1986, and the Ph.D. degree from the Delft University of Technology, Delft, The Netherlands, in 1998. He is currently an Associate Professor with the Circuits and Systems Group, Delft University of Technology. His research interests include wireless communication, particularly narrowband multiuser detection, digital modulation techniques, channel modeling, diversity techniques, and ultra wideband communications and positioning.